SYNCHRONIZED MATERIAL DEPOSITION RATE CONTROL WITH PATH VELOCITY ON FUSED DEPOSITION MACHINES

by

Deniz Sera Ertay

B.Sc., Istanbul Technical University, Turkey, 2014

A THESIS SUBMITTED IN PARTIAL FULFILLMENT OF

THE REQUIREMENTS FOR THE DEGREE OF

MASTER OF APPLIED SCIENCE

in

THE FACULTY OF GRADUATE AND POSTDOCTORAL STUDIES

(MECHANICAL ENGINEERING)

THE UNIVERSITY OF BRITISH COLUMBIA

(Vancouver)

January 2017

Abstract

Additive manufacturing (AM) technologies are used in three-dimensional (3D) printing of parts by depositing the material layer-by-layer on the computer numerical controlled machine tools. While laser and electron beam guns are used to melt, and deposit the metals, thermoplastic materials are heated and deposited by the extruders. When the material deposition is not synchronized with the tangential velocity of the machine, an excess material is accumulated at sharp curvatures where the machine slows down.

This thesis presents a novel algorithm for the synchronized deposition of thermo-plastic materials with the tangential path velocity of the machine under constant temperature. The temperature of the thermoplastic filament needs to be kept at a constant temperature (i.e. 220 Celsius) in a heater chamber. The transfer function between the temperature and current input to the heater is modeled as a first order system whose parameters are time varying as a function of material's extrusion rate. An adaptive pole placement controller is designed to maintain the temperature of the material by manipulating the current supply to the heater as the extrusion rate vary.

The tool path is first smoothed by a fifth order B-spline. The tangential path velocity is also smoothed by a third order spline while respecting heater's power limit as well as the jerk, acceleration and velocity limits of two drives which are used in printing the material layer by layer.

The extrusion rate is controlled proportional to the tangential path velocity while keeping the temperature of the deposited thermo-plastic material at the desired temperature by adaptively controlling current supply to the heater.

The experimentally proven algorithm leads to more uniform material deposition at sharp curvatures and resulting improved dimensional accuracy of printed parts. The proposed methodology can be extended to laser and electron beam based metal printing applications.

Preface

This thesis is a product of the research of the author, Deniz Sera Ertay, under the supervision of Professor Yusuf Altintas. This work has been accomplished in the Manufacturing Automation Laboratory at the University of British Columbia.

A version of Chapter 3 and Chapter 4 has been submitted to Journal of Additive Manufacturing [Ertay D.S., Yuen A, Altintas Y. Synchronized Material Deposition Rate Control With Path Velocity On Fused Deposition Machines, Journal of Additive Manufacturing]. I was the lead investigator, responsible for the major development of the algorithms, analysis, and manuscript composition. Yuen A was involved in experimental setup and contributed to the manuscript edits. Altintas Y was the supervisory author on this project and was involved throughout the project in concept formation and manuscript composition.

Table of Contents

Abstract ..... **ii**

Preface ..... **iv**

Table of Contents ..... **v**

List of Figures ..... **viii**

Nomenclature ..... **x**

Acknowledgements ..... **xvi**

Chapter 1: Introduction 1

Chapter 2: Literature Review 9

2.1 Overview 9

2.2 CAD – CAM of FDM Operations 10

2.3 Process Planning for FDM Operations 12

2.4 Temperature Model of FDM Operations 15

2.5 Conclusion 17

Chapter 3: Coordination of Positioning and Material Deposition in FDM 18

3.1 Overview 18

3.2 CAD-CAM for Additive Manufacturing 19

3.3 Review of B-Splines 20

3.4 Parametric Spline Fitting 23

3.5 Feed Correction Polynomial 25

3.6 Feedrate Optimization 29

3.7 Synchronizing Material Extrusion Rate with Tangential Feedrate 33

3.8 Conclusion 36

Chapter 4: Adaptive Temperature Control of FDM Heater System 37

4.1 Overview 37

4.2 Heating System of FDM 39

4.3 Transfer Function of the FDM Heater 40

4.4 Controller Design 45

4.5 Conclusion 50

Chapter 5: Printing Simulations and Experiments 52

5.1 Overview 52

5.2 Experimental Setup 52

5.3 Experimental Results for the Extrusion Rate Profile 56

5.4 Temperature Model Validation 59

5.5 Conclusions 62

Chapter 6: Conclusions 63

6.1 Conclusions 63

6.2 Future Research Directions 64

Bibliography 66

List of Figures

Figure 1.1 Fused Deposition of Thermoplastic filaments 3

Figure 1.2 Excessive Deposition at Sharp Curvatures 5

Figure 1.3 Chord length and extrusion amount between two consecutive points 6

Figure 1.4 Flow Diagram of the Thesis 8

Figure 3.1 Spline Fitting 21

Figure 3.2 Synchronized Tangential Path Velocity and Extrusion Rate 35

Figure 4.1 The Change in Temperature with Extrusion Rate 38

Figure 4.2 Experimental Identification 44

Figure 4.3 Heating System of FDM Machine 46

Figure 4.4 Controller Parameters 48

Figure 4.5 Adaptive control of temperature as the extrusion rate changes along the tool path. a) Current command history b) Transient change of the temperature before the extrusion and steady state temperature control after the extrusion starts. 49

Figure 4.6 Adaptive control of temperature as the extrusion rate remains the same along the tool path. a) Current command history b) Transient change of the temperature before the extrusion and steady state temperature control 50

Figure 5.1 Experimental Setup 53

Figure 5.2 Spline Fitting on Toolpath Points 55

Figure 5.3 3D Parts Printed in the Experiments (3D CAD Part (a) and 3D Printed Part (b)) 56

Figure 5.4 Deposition Profile Comparison between Constant Extrusion Rate (a) and Synchronized Extrusion Rate (b) 57

Figure 5.5 3D Laser Scan of Two Curves of the Part with constant (a) and synchronized (b) extrusion rates 58

Figure 5.6 Comparison of Experimental Results Printed with Constant Extrusion Rate (a) and Synchronized Extrusion Rate (b) 61

Nomenclature

A_{eq}	Equivalent area between the filament material and heating coil
A_f	Final cross section area of the filament (after deposition)
A_i	Initial cross section area of the filament (before deposition)
$A_k^f, \mathrm{B}_k^f, \ldots, \mathrm{H}_k^f$	Coefficients of the feed correction polynomial
A_{PLA}	Cross section area of the PLA filament
E_{in}	Heat energy provided by the heating coil
E_{out}	Heat energy loss due to the filament material flow through the aluminum heating block
E_{stored}	Net heat energy stored in the aluminum block
$\dot{E}$	Extrusion rate of the filament
$\mathrm{J}_{x,\max}, \mathrm{J}_{y,\max}$	Jerk limits of the x and y axis
L_{eq}	Equivalent length between the filament material and heating coil

$N_{i,n}$	Blending functions of the B-Spline
$P(u)$	Geometric B-Spline
Q_n	Position coordinates
$\dot{Q}, \ddot{Q}, \dddot{Q}$	The feedrate, acceleration and jerk profiles as a function of the toolpath displacements
$R(z^{-1}), \mathrm{r}_0, \mathrm{r}_1, \ldots, \mathrm{r}_p$	Error regulator of the PP controller and its parameters
R_h	Resistance of the heater coil
$S(u)$	Geometric polynomial spline
$S(z^{-1}), s_0, s_1, \ldots, s_f$	Feedback regulator of the PP controller and its parameters
S_k	Total length of the toolpath
$T(z^{-1}), \mathrm{t}_0$	Feedforward regulator of the PP controller and its parameter
T_A	Actual (measured) printing temperature
T_i	Initial temperature of the filament
T_R	Reference printing temperature

T_s	Sampling time of the servo system
T_Σ	Total travel time of the toolpath
U	Knot vector of the geometric B-Spline
V_f	Final linear velocity of the filament (after deposition)
V_i	Initial linear velocity of the filament (before deposition)
V_t	Tangential path velocity of the extruder head
$\dot{V}_f$	Final volumetric flow of the filament (after deposition)
$\dot{V}_i$	Initial volumetric flow of the filament (before deposition)
$a_n, a_{n-1}, \ldots, a_0$	Coefficients of the nth geometric spline
$\mathrm{a}_{x,\max}, \mathrm{a}_{y,\max}$	Acceleration limits of the x and y axis
c_{Al}	Specific heat capacity of aluminum
c_{PLA}	Specific heat capacity of the PLA filament
c_h	Specific of the heater coil
d	Chord length between two consecutive points

d_f	Final diameter of the filament (after deposition)
d_i	Initial diameter of the filament (before deposition)
e	Prediction error of the feed correction polynomial
f_i	Feedrate control points
k_{Al}	Thermal conductivity of aluminum
m	Degree of the geometric B-Spline
m_{Al}	Mass of the aluminum block
m_h	Mass of the heater coil
$\dot{m}$	Mass flow rate of the filament
p_i	i^{th} position point
q_n	Control point coordinates
$\dot{s}, \ddot{s}, \dddot{s}$	The tangential feedrate, acceleration and jerk profiles (i.e. first, second and third derivatives of the displacement with respect to time)
u	Geometric spline parameter

$\hat{u}(s)$	Feed correction polynomial
$\hat{u}(\sigma)$	Normalized feed correction polynomial
Δu	The increment in spline parameter between two consecutive points
$\bar{u}_k$	Parameter values assigned to tool tip position vectors p_k
$\hat{u}_s, \hat{u}_{ss}, \hat{u}_{sss}$	First, second, and third derivatives of the feed correction polynomial with respect to displacement s
$v_{x,\max}, v_{y,\max}$	Velocity limits of the x and y axis
$x_s, y_s, x_{ss}, y_{ss}, x_{sss}, y_{sss}$	Feedrate, acceleration and jerk profiles of each axis
z_1, z_2	Desired closed loop poles in discrete time domain
σ_M	Normalized arc displacement
η_{heff}	Heater efficiency coefficient covering the energy loss to the environment
ρ_{PLA}	Density of the PLA filament
μ	Ratio of final linear velocity of the filament to tangential federate
ABS	Acrylonitrile Butadiene Styrene

AM	Additive manufacturing
B-Spline	Basis spline
CAD	Computer aided design
CAM	Computer aided manufacturing
CNC	Computer numerical control
FDM	Fused deposition modeling
FE	Finite element
NURBS	Non-uniform rational basis spline
PID	Proportional integral derivative controller
PLA	Polylactic Acid
PP	Pole placement controller
STL	Stereo Lithograph

Acknowledgements

I am most grateful to my research supervisor Dr. Yusuf Altintas, who provided me valuable guidance, unlimited support, and encouragement throughout my graduate study. It has been a great pleasure learning from him and being an assistant to him. I very much appreciated having the opportunity to work with him and to make my first steps into the academic world under his supervision.

I would like to thank Dr. Doruk Merdol, who initiated this journey and believed in me and I would also like to give many thanks to my colleagues in the Manufacturing Automation Laboratory for their willingness to share their knowledge and experience with me. I particularly wish to thank my friend Alex Yuen for his valuable assistance in carrying out my experiments. I have been extremely lucky to have had the unconditional support, encouragement and friendship of my sister by heart, who is miles away, Ceren Demirbag.

Finally, I am very thankful to have had the support of my family behind me. Many thanks and much gratitude to my mother Semra, my father Bahadir and to my brother Levent. I thank my parents for teaching me the importance of education and knowledge, for making so many sacrifices for my education and for raising me to be a strong woman. I am very proud to be their daughter and I dedicate my thesis to my beloved parents.

This research is supported by NSERC Strategic Research Grant (STPGP 493727) led by Prof. Chad Sinclair and NSERC Discovery Grant of Prof. Yusuf Altintas.

Chapter 1: Introduction

Additive manufacturing (AM), which is often called as three-dimensional (3D) printing, is a manufacturing process based on layer-by-layer deposition of materials under a computer controlled system. It has been a rapidly advancing technology with wide applications in manufacturing biomedical and mechanical parts. AM systems slice the 3D model of the part into layers with a desired thickness in a Computer Aided Design (CAD) system. A tool path is generated to trace each layer and supplied to Computer Numerical Controlled (CNC) machine to print the part layer by layer. Additive manufacturing can be extrusion, sintering or jetting based depending on the material to be used and the mechanical property requirements of the part. While the metals are melted using either laser or electron-beam energy, the thermoplastic materials are heated to create liquids that can be extruded with syringes. The molten materials are printed along the tool path layer by layer. Highly complex geometries can be printed layer by layer, and the accuracy of the part depends on the control of material deposition rate and process.

A variety of materials such as metals, plastics, and ceramics can be used in additive manufacturing with different initial states like powder, liquid and filament. Although every kind of additive manufacturing processes have their own advantages and disadvantages over each other, they have some characteristic advantages in common such as allowing complex design, decreasing the lead time, avoiding the need for tool change through the process, enhancing an

easier process planning, minimizing the need for parts assembly and minimizing the waste of material. Their common disadvantages are the poor surface finish, the risk of warpage and low tensile strength of the material in longitudinal direction. However, with the recently intensified research efforts, AM technology has been rapidly advancing with the applications ranging from biomedical implants and cells, to metallic parts used in consumer and aerospace industries.

The most common application of additive manufacturing is rapid prototyping, which is called Fused Deposition Modeling (FDM) and developed by Stratasys [1]. It is based on extrusion of thermoplastics such as Polylactic Acid (PLA) and Acrylonitrile Butadiene Styrene (ABS), which are in a filament form with a diameter of 1.75 mm or 2.85 mm. The filament is fed into the extruder with the help of two reciprocal gears shown in Figure 1.1, which are driven by a stepper motor. Close to the extruder tip there is the part called the hot-end, which consist of the heater, the nozzle, the finned cylinder and the fan. The filament is heated up to its melting point (200-230 ^{o}C) at the heater chamber whose temperature is monitored with a thermocouple or thermistor. The temperature is kept at the set value by controlling the current supplied to the heater. The heated filament becomes liquid, and extruded through a nozzle whose output diameter determines the dimensional resolution of the printing process. The most common nozzles have diameters varying from 0.2 to 0.5 mm. The fan and the fins are used to distribute the heat along the filament more uniformly to avoid clogging of the nozzle and the extruder.

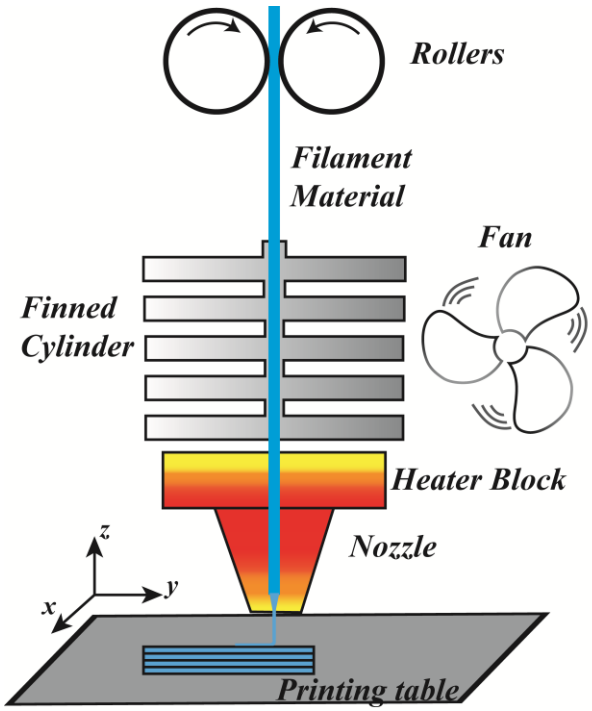

Figure 1.1 Fused Deposition of Thermoplastic filaments

3D CAD model is created and sliced into layers with a specified thickness. The cross-sectional area at each slice defines the toolpath. The most common tool path generation method is to contour the cross-sectional area and do the infill with required fill pattern and density. The extrusion rate is determined depending on the machine, heater and extrusion capacity. The tool path is generated as machine G-codes that consist x-, y-, z-axis position commands, feedrate for the table motion and the extrusion rate.

The main process parameters for FDM processes are number of layers or layer height, feedrate (table speed), extrusion rate, printing temperature, infill pattern and density, support material (if necessary). These properties have their own effect on the dimensional and surface

quality of the part. The quality of the printed part depends on layer height, extrusion rate and also the positioning accuracy of the machine. The height of the first layer is usually higher than the other layer heights but it still needs to be lower than the nozzle diameter in order to provide the sticking of the first layer on the printing surface. The bonding quality between consecutive layers, which defines the tensile strength along the longitudinal direction of the printed part, is also dependent on the layer height and temperature.

The quality of the printed part also depends on how well the extruder and motion control of the printing table are synchronized. It is almost impossible to keep the feedrate of the printing table constant through the whole toolpath, which will have fluctuations depending on the toolpath geometry. The machine slows down or stops momentarily at the sharp corners and curvatures to reduce the contour errors contributed by the limited bandwidth of the feed drives. If the extruder deposits the material at a constant rate, there will be over-deposition at the sharp curvatures as shown in Figure 1.2 which will lead to inaccurate printing of the part. The extrusion rate needs to be synchronized with the feedrate to avoid depositing irregular material rates along the curved tool paths.

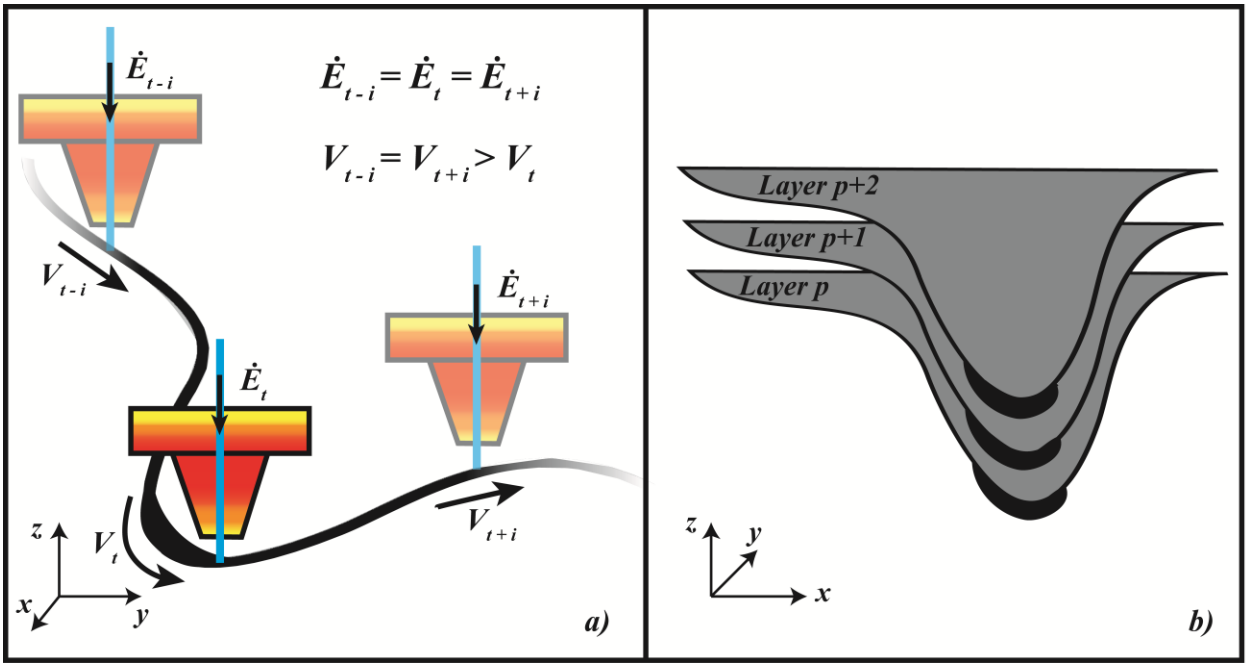

Figure 1.2 Excessive Deposition at Sharp Curvatures

The extrusion rate is determined by the chord length between two consecutive points along the tool path as shown in Figure 1.3. However, a linear relationship between the chord length and material deposition rate does not lead to a uniform material printing along the curved paths. The problem is more complex in laser and electron-beam based processes where the control parameters such as beam speed, beam intensity, melt pool size and sintering of the metal powder affect the deposition process.

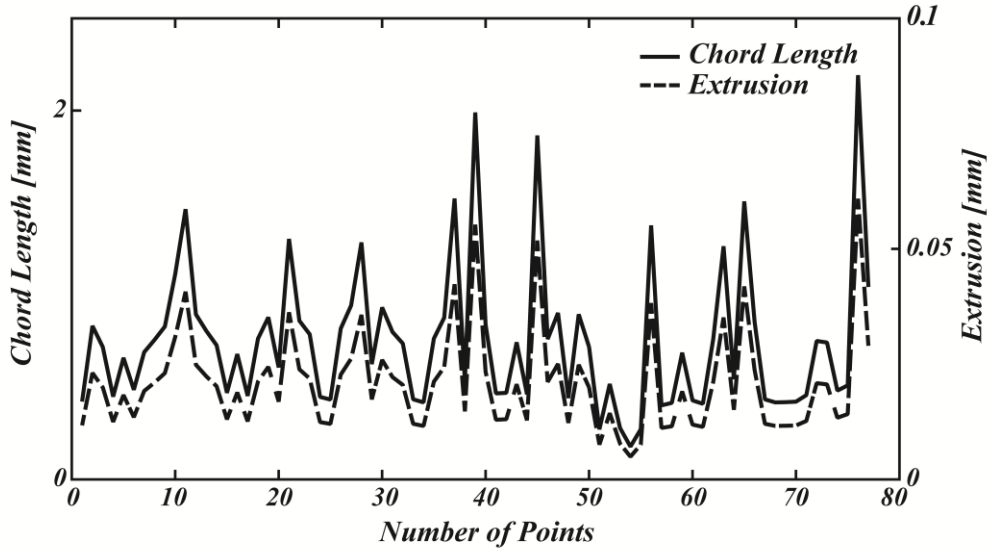

Figure 1.3 Chord length and extrusion amount between two consecutive points

Synchronizing the extrusion rate to feedrate will also bring some fluctuations in the extrusion rate profile. The amount of material to be extruded and travelling through the heater block will vary with time while the heat energy transferred to the filament remains the same, which will lead to overheating of the material. The heater temperature must be kept at a constant level by considering the extrusion rate of the material.

This thesis presents a set of algorithms which lead to uniform material deposition along the curved tool paths. The tool path is first smoothed with a fifth order B-spline to avoid sharp discontinuities. The trajectory is planned with a feedrate optimization algorithm, where the cycle time of the process is minimized by considering the machine and the extruder's heating capacities. The feed decreases at sharp curvatures and accelerates afterwards according to the

tangential and axis velocity, acceleration and jerk limitations. The extrusion rate is kept proportional to the tangential path velocity to deposit uniform material along the curved tool path. The heating system of the extruder is modeled as a function of the extrusion rate and an adaptive pole placement controller is designed in order to keep the temperature at the desired level. The proposed method is experimentally illustrated by printing a part with highly complex curvatures.

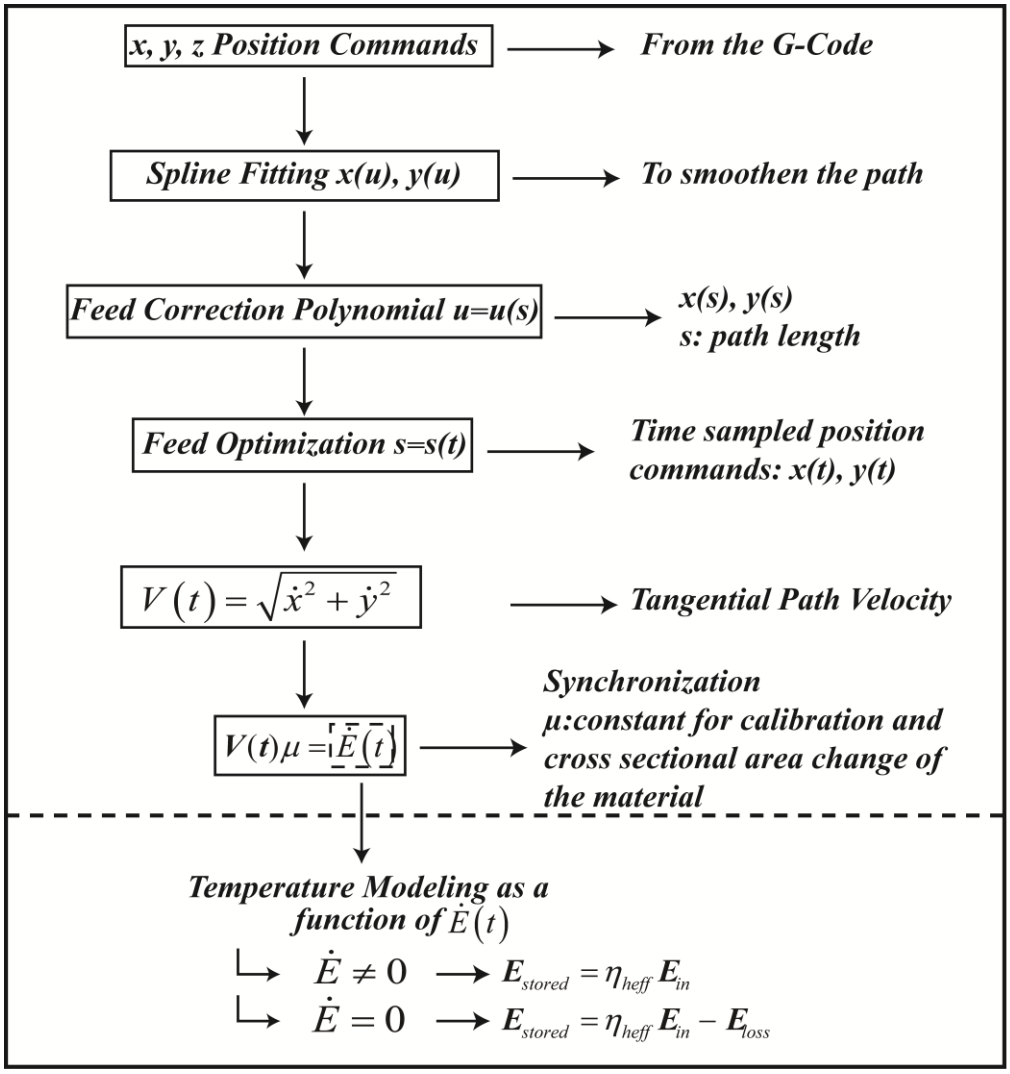

Figure 1.4 Flow Diagram of the Thesis

The thesis is organized as follows: the relevant literature is reviewed in Chapter 2. The synchronization of the extrusion rate with the tangential path velocity is presented in Chapter 3. The adaptive temperature model as a function of extrusion rate is described in Chapter 4. The experimental setup and experimental results are shown in comparison with the simulation results in Chapter 5. The conclusions and future research directions are discussed in Chapter 6.

Chapter 2: Literature Review

2.1 Overview

Additive manufacturing has been an active research area, since its application areas expanded due to the flexibilities and the advantages of the process. The process is being rapidly adopted by industry due to its advantages such as easy process planning, low setup time over conventional manufacturing processes, and possibility of creating complex shapes. The research on additive manufacturing is mostly focusing on CAD and CAM of the process. As the biggest disadvantage of creating parts with layer-by-layer is the poor surface finish, there is a need for research in toolpath planning and slicing algorithms. Most of the commercial FDM machines are using linear interpolation, whereas high speed CNCs are using linear, circular and spline interpolators. Adaptive slicing algorithm [2] is proposed to improve the surface finish such as decreasing the layer height at geometrically complex areas of the part. Smooth toolpath generation algorithms are proposed so that a machine can give good surface finish with a linear interpolator. There are also articles [3] based on the aim of improving the mechanical properties of the part such as the tensile strength.

There is a need for the process planning of process parameters such as layer height, extrusion rate, temperature, and material and extruder properties. Manufacturers are using trial

and error to set these parameters or they are using the supplier suggestions. However, each part requires a process planning, which fits into the design properties.

Temperature modeling of additive manufacturing systems are more focused on metal parts because it has a more effect on part's strength and surface finish. In FDM processes temperature modeling also plays a role in surface finish. The over-heated parts of the filament tend to lose their shape more as they are softer after deposition [4]. Furthermore, there could be an inhomogeneous temperature distribution through the printed part. Overheated material can cause warping after or during the process. On the other hand, under-heated material can cause nozzle clogging and sticking problems between two consecutive layers of the part [4]. The sticking problem can result in low tensile strength of the part in its longitudinal direction, or there might be no connection between the layers at all. In order to overcome these problems, it is necessary to keep the temperature constant at the heating block by designing a proper controller.

2.2 CAD – CAM of FDM Operations

The 3D part is generated in a CAD software and converted into an STL (Stereo Lithography) file. For the CAM operations Slic3r is used in this thesis, which is an open source CAM software for FDM applications. It slices the part in STL format according to the defined layer height. Ma et al. proposed an adaptive slicing algorithm by fitting a NURBS (Non-uniform Rational Basis Spline) to the surface profile of the part in order to achieve a better surface finish and keep the process as efficient as possible [5]. There are more examples of slicing algorithms

to improve the surface finish and increase the productivity for FDM operations [6]. Advanced slicing algorithms are also used to improve the part accuracy [7]. It is necessary to decrease the layer height in printing complex geometries with sharp curvatures. However, decreasing the layer height will increase the cycle time of the process. Ghazanfari et al. investigated the problem of part inaccuracy due to horizontal staircase effect [8]. They modeled the optimal rastering orientation in order to estimate and minimize the inaccuracy. The staircase effect is discussed by Kim et al. and suggested to add 2 degrees of freedom (DOF) to print a curved surface accurately with a synchronized and smooth motion of the axes [9].

After the slicing operation, the toolpath is given for each layer according to the infill density, infill pattern and contour perimeters. It can be said that for a 100 % infill density contour perimeters as an infill pattern is the most productive one. It usually has less sharp corners and there would be less full stops. There are articles, which investigated optimization of the cycle time of the process by choosing proper infill density and pattern regarding the part's tensile strength [10]. Topology optimization is also done for the efficient use of the material. Toolpath commands are given in a linear motion commands in the form of G-Codes as the commercial FDM machines are using only linear interpolators for the table motion. Heller et al. worked on improving mechanical properties by adding fibers to the material and used an FE (finite element) model to evaluate the polymer melt flow and fiber orientation by considering the nozzle geometry and the flow [11].

There are more examples of toolpath smoothing in high speed CNC literature. The fast changes of feedrate could result in high acceleration and jerk values [12]. To overcome these

problems there are path smoothing algorithms proposed by Wang and Yang [13] by fitting a geometric spline. It assumes that $du = ds$ at the middle point of the spline segment, where u is the geometric spline parameter and s is the path displacement. It uses a third order spline with C^2 continuity resulting in reductions in feedrate fluctuations. In a later study, Wang et al. improved the algorithm by arc-length parametrized C^3 quintic splines [14]. Farouki and Sakkalis show that $du = ds$ is not possible mathematically, when there are sharp curvatures in the toolpath [15]. They proposed using Pythagorean Hodograph curves by computing the arc-length analytically. Furthermore, Erkorkmaz and Altintas defined a nonlinear relationship between the spline parameter and the displacement by using a 7th order polynomial [16]. They expressed the spline parameter u as a function of displacement with a polynomial, which is reducing the fluctuations in the feedrate profile.

2.3 Process Planning for FDM Operations

The CAM software for FDM operations gives a G-Code, which includes the toolpath positions, feedrate for the table motion, desired printing temperature and extrusion rate commands. The maximum feedrate and extrusion rate values are defined by the user in the software. The commands in the G-Code for the feedrate and extrusion rate are calculated point-to-point depending on the chord length between two consecutive points.

There has been some work reported to avoid excessive material deposition at the critical points of complex parts and to obtain a homogeneous deposition profile. Bellini et al. proposed a

feedrate control system to keep the volumetric flow rate constant Q. They defined a linear relationship between the volumetric flow rate and the feedrate [17]. It is a real-time system that measures the table speed and adjusts the extrusion rate so that the ratio of these two will remain the same. However, they have only shown the simulation results. W represent the desired rod width, H is the slice thickness and v is the linear velocity of the extruder head.

$$v = \frac{Q}{WH} \tag{2.1}$$

However, they assumed a 100 % efficiency between extrusion rate and feedrate. Agarwala et al. [18] shows that the efficiency shouldn't assume a 100 % efficiency because the rollers could be worn out or high pressure drop could appear at the nozzle.

Yardimci et al. [19] considered the buckling effect as a limitation factor. The buckling of the filament could result in nozzle clogging. This can happen at high printing temperatures, under high pressure torque transmitted from the rollers and in the case, where the fan is not working. Yardimci and Guceri [20] also took the nozzle geometry into account, where Ramanath et al. [21] and Mostafa et al. [22] just assumed that the nozzle is a straight cylindrical tube. Liang et al. [23] investigated the impact of nozzle geometry and the issue of nozzle clogging, which is caused by instabilities in the extrusion process.

Weiss [24] pointed out that there is a need for a model, which overcomes the problem of excessive material deposition at sharp corners and high curvatures. Bouhal et al. [25] modeled a tracking control with a feedforward method in order to minimize the tracking error and excessive

deposition. Han and Jafari [26] proposed a toolpath based deposition planning, where groups of similar lengths of toolpath vectors are put together and a desired deposition rate is given to each group by using grouping and mapping algorithms. Han and Jafari [27] indicated that the ratio between roller speed and tangential feedrate should be kept constant. They proposed a filament extrusion system, where the extrusion rate is regulated according to the head speed in real time. However, the filament extrusion system is an open loop system and there is no experimental validation of this technique.

There are also extrusion rate planning techniques regarding to the issues of spreading, bonding and adhesion of the material. Crockett [28] modeled a Hagen-Poiseuille flow considering the printing nozzle geometry and the viscosity of the material melt. Middleman [29] modeled the maximum extrusion rate in order to have a continuous flow. As the extrusion rate is considerably high or low, the flow could go unstable and discontinuous. The bonding between two consecutive layers affects the tensile strength of the printed part in its longitudinal direction. Bellini and Guceri [30] mention that the bonding would be better, if the time between depositions of two consecutive layers is short enough. So, that the temperature will stay high longer to improve the bonding. In order to investigate the bonding properties, it is necessary to have the temperature distribution of the material until the next layer comes on top of it. Thomas and Rodriguez [31] presented a 2D model, which predicts the temperature history of the filament depending on the printing shape and printed filament geometry. Bellini [32] proposed the lumped capacity model, which predicts a steady temperature drop over time. It shows good results at short times after extrusion compared to the experimental results.

There are also articles which investigated the relationship between material deposition and table speed in metal additive manufacturing with laser and electron beams. The process involves more control parameters than in FDM such as melt pool size, sintering, beam density and beam speed. Hu and Kovacevic designed a feedback controller to manipulate the laser power while keeping the laser scanning and powder feed constant [33]. The aim was to build a uniform shape by keeping a uniform melt pool. Smichi performed experiments in order to define the relationship between the sintering rate and densification of the metal powder by considering laser power, scan rate and layer thickness as variables [34]. A similar work by NIST shows the effects of process parameters on product quality [35], where their main aim is to develop an online measuring system for laser and electron beam aided additive manufacturing.

In this thesis, an extrusion rate planning method is proposed in order to avoid excessive deposition at critical points such as sharp corners and high curvatures. The toolpath geometry is considered in the trajectory planning. The tangential velocity decreases at sharp corners and high curvatures according to the machine axis limitations such as velocity, acceleration and jerk. After the trajectory planning a linear relationship is used between tangential velocity and the extrusion rate in order to have a homogeneous deposition profile through the entire toolpath.

2.4 Temperature Model of FDM Operations

A model is needed for FDM operations in order to keep the temperature consistent through the process. Commercial FDM machines usually uses PID (Proportional Integral

Derivative) controller to control the temperature, and keep it at the commanded temperature all the time. Extruder manufacturers are also recommending to use PID controller for the heater by just giving the controller parameters $\left(K_p, K_i, K_d\right)$.

FE analyses are used to predict the temperature of the filament during and after the extrusion. The analysis is used to investigate the bonding between two consecutive layers of the part, to analyse the melt fluid dynamics and to see the temperature distribution after the extrusion process in order to minimize the risk of warping of the part as it is mentioned in the previous section. Ji and Zhou [36] presented an analyses of the melt fluid dynamics and heat transfer at the heater with the FE method. Ramanath et al. [21] worked on the effect of temperature on pressure drop prediction by using the FE method and compared it with their analytical model. Although the FE analyses predict the temperature in the filament, it is hard to validate the models experimentally, as it is almost impossible to measure and collect a history of the temperature values of a certain point of the filament.

Bellini et al. [17] proposed a mathematical model for liquefier dynamics by focusing on extrusion rate, the flow at the nozzle, and also the relationship between heat flow rate and extrusion rate is defined, which is the average temperature and it is considered regardless of its location. They also showed that a sudden change in extrusion rate causes a sudden change in the temperature of the filament. A transfer function approach has been investigated for the liquefier dynamics. The system is identified only experimentally, which means that the model depends on a certain application, filament type and extruder.

There has been no work so far that the temperature is modeled as a function of the extrusion rate. Most of the energy loss occurs due to the moving mass, where the material absorbs the heat. In this thesis, an analytical temperature model is presented, where its dynamic behaviour is changing according to the extrusion rate at each step. It is important to avoid the fluctuations in the extrusion rate profile. The temperature loss at each time step would be different because the mass passing through the heating block per unit time is different.

2.5 Conclusion

In this chapter a review of relevant literature is presented in additive manufacturing about CAD-CAM operations of the process, process planning and control and temperature modeling of the liquefier. Although there haven't been many works on extrusion rate planning and temperature modeling, an overview is given what the literature focused on additive manufacturing. The effectiveness and advantages of the methods represented in the literature are discussed. The current techniques used in FDM technology are also given. Their lack of process control and needs for a better part quality are shown. The originality and benefits of the methods proposed in this thesis are expressed by comparing them with the relevant literature is given.

Chapter 3: Coordination of Positioning and Material Deposition in FDM

3.1 Overview

FDM process starts with digital modeling of the 3D object in a CAD software. After the CAM operations, the G-code is taken and supplied to the machine with the information of toolpath positions, feedrate and extrusion commands. A 3D object with a complex geometry is also hard to print at the curvatures and sharp corners, depending on the machine limitations. The machine will slow down or make a full stop at the curvatures or sharp corners in order to keep the tracking error at its minimum and follow the toolpath more accurately.

When there are fluctuations in the trajectory profile because of the complex toolpath geometry, the extrusion rate remains constant and keeps feeding material through the nozzle. As the extruder will spend more time on the curvatures and sharp corners, there will be excessive material deposition, which results in a poor deposition profile and surface finish. In order to avoid excessive and non-uniform material deposition, the extrusion rate must be kept proportional to the tangential velocity.

In this chapter, the current technology of CAD-CAM in additive manufacturing is explained first. The B-spline spline fitting is described, and the feedrate planning is explained. The relationship between the feedrate and extrusion rate is demonstrated.

3.2 CAD-CAM for Additive Manufacturing

The geometric model of a part is created in a CAD software and converted into an STL file, where the 3D CAD model is meshed into triangular elements. The size of the triangular elements has an effect on how accurately and precisely the 3D object is manufactured layer by layer. There are some software, where the CAD and CAM for additive manufacturing can be carried out together. However, in this thesis Siemens NX Unigraphics is used to create the 3D object, converted into an STL file. Open source Slic3r CAM system is used for additive manufacturing and especially for FDM processes.

It is possible to set the layer height, infill pattern and density, feedrate, support material and some properties in the CAM system. The printing temperature, the diameter of the filament and the fan properties are set. Printer setting indicate the printing bed shape, the extruder nozzle diameter can be defined for post-processing of the tool path for a specific machine.

The G-Code from Slic3r contains the toolpath positions, the table speed and the extrusion commands. However, the extrusion commands are given in each line as extrusion length in mm. The extrusion rate is defined and fixed in the CAM software before generating the G-Code Keeping the extrusion rate constant through the entire toolpath could be good enough to print simple geometries with less curvatures and sharp corners, where feedrate fluctuations are minimal. Extrusion commands, which are corresponding to extrusion lengths, are calculated proportional to the chord length between two consecutive points in the toolpath. However, the

chord length ($L_i = \sqrt{(x_{i+1} - x_i)^2 + (y_{i+1} - y_i)^2}$) is not always equal to the path length, especially at curved paths.

The extrusion commands are planned without considering the geometry (the curvatures and sharp corners) of the toolpath. This problem will result in inhomogeneous extrusion profile through the complex geometries and will lead to poor surface finish and dimensional errors. In order to avoid this problem, the motion of the table should be smoother and so as the toolpath. B-spline is fit to the position commands received by the CAM system. and a jerk continuous kinematic profile is planned while considering the machine's limits and the geometry of the toolpath.

3.3 Review of B-Splines

Splines are used to smooth the discontinuous kinematic profiles and fluctuations along the paths. Non-Uniform Rational Basis Splines (NURBS) and Basis Splines (B-splines) are polynomials to smooth tool-paths with local modifications. A spline can be represented by a polynomial as follows:

$$S(u) = a_n u^n + a_{n-1} u^{n-1} + \ldots + a_0 \tag{3.1}$$

The tool path is assumed to pass through *m+1* number of points defined by a vector array as:

$$\mathbf{p} = \{ p_0 \quad p_1 \quad \cdots \quad p_i \quad \cdots \quad p_m \} \quad \leftarrow p_i(x_i, y_i) \tag{3.2}$$

B-splines can be considered as a simplification of NURBS and in this thesis a fifth order (*n=5*) NURBS spline is fitted to tool path points $\mathbf{p}$ to have geometric jerk continuity:

$$P(u) = \begin{bmatrix} x(u) \\ y(u) \end{bmatrix} = \sum_{i=0}^{m} N_{i,n}(u) P_i \quad \leftarrow u \in (0,1) \tag{3.3}$$

where $N_{i,n}(u)$ and P_i are the blending function and the control point, respectively. The B-Splines still has the flexibility of local modifications in the curve.

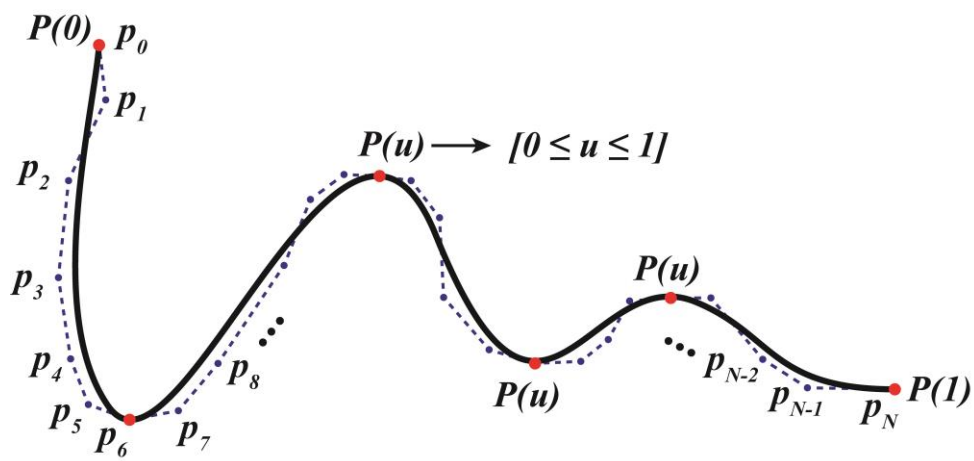

Figure 3.1 Spline Fitting

The characteristics of the B-splines are determined by the knot vector *U*, the number of control points and the degree of the spline. The general distribution of the spline is shown by the

knot vector within the parameter interval $u \in [0,1]$. The knot vector is a set of real numbers, which consist of non-decreasing integers:

$$U = [0,\ldots,0,u_{n+1},\ldots,u_{n+1+m},1,\ldots,1] \tag{3.4}$$

where $m+1$ is the number of the control points through the B-Spline. There will be n+1 times zeros and ones at the beginning and at the end of the knot vector, respectively, in order to force the first and the last control point (P_0, P_m) to be the initial and end points of the spline. If the knot vector and the degree of the curve are known, the blending functions can be evaluated. The blending functions are calculated starting from the zero degree blending functions:

$$N_{i,0}(u) = \begin{cases} 1 & u \in [u_i, u_{i+1}) \\ 0 & u \notin [u_i, u_{i+1}) \end{cases} \tag{3.5}$$

Higher degree blending functions are calculated recursively:

$$N_{i,n}(u) = \frac{u - u_i}{u_{i+n} - u_i} N_{i,n-1}(u) + \frac{u_{i+n+1} - u}{u_{i+n+1} - u_{i+1}} N_{i+1,n-1}(u) \tag{3.6}$$

The position coordinates of the spline can be found and represented by the sum of the products of the blending functions and control points.

$$P(u) = N_{0,n}(u) \cdot P_0 + N_{1,n}(u) \cdot P_1 + \ldots + N_{m-1,n}(u) \cdot P_{m-1} + N_{m,n}(u) \cdot P_m \tag{3.7}$$

The smoothness of the curve is determined by the degree of the blending functions. If there is a need for third order (jerk) continuity in the toolpath to have a smooth trajectory, the first, second and the third derivatives of the spline should be known. The derivatives will be a function of blending function's parameter *u* since the control points are constant coefficients in the B-Spline equation.

3.4 Parametric Spline Fitting

For a set of given position points Q_k (k=0, 1…m) a nth degree B-spline curve can be interpolated to these points. The main aim is to find the control points by knowing the degree of the curve, the position points and the knot vector.

$$Q_k = C(\bar{u}_k) = \sum_{i=0}^{m} N_{i,\mathrm{n}}(\bar{u}_k) P_i \tag{3.8}$$

where P_i are the $(m+1)$ unknown control points, $N_{i,n}$ are the nth degree B-spline blending functions. A spline parameter value u_k, which lies in the range $u \in [0,1]$, is assigned to a Q_k and an appropriate knot vector should be selected. The centripetal method is used for assigning u_k to Q_k when the data includes sharp corners. The distribution of the position vector along the toolpath is used to assign the parameter values in this method.

$$
\begin{aligned}
&d = \sum_{k=1}^{n} \sqrt{|Q_k - Q_{k-1}|} \\
&\bar{u}_0 = 0 \qquad\qquad \bar{u}_n = 1 \\
&\bar{u}_k = \bar{u}_{k-1} + \frac{\sqrt{|Q_k - Q_{k-1}|}}{d}, \ \mathrm{k} = 1, \ldots, \mathrm{N}-1
\end{aligned}
\tag{3.9}
$$

The distribution of the position points along the toolpath determines the assignment of the parameter values. The centripetal method minimizes the fluctuations in the spline between two consecutive points. Further details can be found in [37].

The number of blending function and control points are set equal to the number of tool tip positions, which gives a $(n+1)x(n+1)$ linear system of equations to be solved for the control points.

$$
\underbrace{\begin{bmatrix} N_{0,p}(\overline{u_0}) & \cdots & N_{N,p}(\overline{u_0}) \\ \vdots & \ddots & \vdots \\ N_{0,p}(\overline{u_N}) & \cdots & N_{N,p}(\overline{u_N}) \end{bmatrix}}_{N} \underbrace{\begin{bmatrix} Q_0^T \\ \vdots \\ Q_N^T \end{bmatrix}}_{Q} = \underbrace{\begin{bmatrix} q_0^T \\ \vdots \\ q_N^T \end{bmatrix}}_{q}
\tag{3.10}
$$

The vector of control points can be found by taking the inverse of N:

$$
Q = N^{-1} q \tag{3.11}
$$

As the control points and the knot vector are known, any point on the B-spline can be represented as a function of blending functions and the control points.

3.5 Feed Correction Polynomial

The relationship between spline parameter *u* and displacement *s* is defined with a feed correction polynomial proposed by Erkorkmaz [16]. It schedules the spline parameter u based upon the displacement in order to minimize the fluctuations in the feedrate profile. A seventh order polynomial is used to define the relationship:

$$\begin{aligned} &\hat{u} = A_k^f s^7 + B_k^f s^6 + \cdots + H_k^f \\ &where: 0 \le s \le S_k \end{aligned} \tag{3.12}$$

The displacement should be calculated first, and it can be expressed with the following integral:

$$\begin{aligned} &s(a) = \int_0^a \left\| P'(u) \right\| du = \int_0^a \sqrt{P_x'^2 + P_y'^2} \\ &where: 0 \le a \le 1 \end{aligned} \tag{3.13}$$

which is difficult to solve analytically. It is solved numerically using Simpson's integration rule with an adaptive bisection technique [38]. It can be represented as:

$$\begin{aligned} &s(b) - s(a) = \int_a^b \sqrt{P'^2_x + P'^2_y} du \approx \frac{b-a}{6}\left[f(a) + 4 f(\frac{a+b}{2}) + f(b) \right] \\ &where: 0 \le a < b \le 1 \\ &\qquad f(u) = \sqrt{P_x'^2 + P_y'^2} \end{aligned} \tag{3.14}$$

As a result the series of displacements are summed up cumulatively and the vector of displacements is built. This vector should be mapped to the vector of spline parameters.

$$u = [0 \quad \Delta u \quad 2\Delta u \quad \cdots \quad M\Delta u]^T \rightarrow s = [0 \quad s_1 \quad s_2 \quad \cdots \quad s_M]^T \tag{3.15}$$

A feed correction polynomial is fit over the arc displacement and corresponding spline parameter values. It is normalized by the total displacement in order to avoid ill conditioning. The polynomial becomes:

$$\begin{aligned} &\hat{u} = a_k^f \sigma^7 + b_k^f \sigma^6 + \ldots + h_k^f \\ &0 \le \sigma \le 1 \end{aligned} \tag{3.16}$$

where $\sigma = s / s_M$, $a_k^f = s_M^7 A_k^f$, $b_k^f = s_M^6 B_k^f$, … , $h_k^f = H_k^f$. Similarly, the first, second and third derivatives with respect to arc displacement are also normalized:

$$\begin{aligned} \hat{u}_s &= \frac{d\hat{u}}{ds} = \frac{1}{s_M}[7a_k^f \sigma^6 + 6b_k^f \sigma^5 + \ldots + g_k^f] \\ \hat{u}_{ss} &= \frac{d^2\hat{u}}{ds^2} = \frac{1}{{s_M}^2}[42a_k^f \sigma^5 + 30b_k^f \sigma^4 + \ldots + 2f_k^f] \\ \hat{u}_{sss} &= \frac{d^3\hat{u}}{ds^3} = \frac{1}{{s_M}^3}[210a_k^f \sigma^5 + 120b_k^f \sigma^4 + \ldots + 6e_k^f] \end{aligned} \tag{3.17}$$

The feed correction polynomial is found with a least square fit over the arc displacements and spline parameter values while maintaining zero, first and second order boundary conditions at both end of the spline segment. The normalized arc displacements in a vector form will be:

$$\sigma = [0 \quad \sigma_1 \quad \sigma_2 \quad \dots \quad \sigma_M]^T = \frac{1}{s_M} s = \frac{1}{s_M}[0 \quad s_1 \quad s_2 \quad \dots \quad s_M]^T \tag{3.18}$$

The corresponding spline parameter predictions obtained with the feed correction polynomial are:

$$\hat{u}_k = \begin{bmatrix} 0 \\ \hat{u}_1 \\ \hat{u}_2 \\ \vdots \\ \hat{u}_M \end{bmatrix} = \underbrace{\begin{bmatrix} 0 & 0 & 0 & \cdots & 1 \\ \sigma_1^7 & \sigma_1^6 & \sigma_1^5 & \cdots & 1 \\ \sigma_2^7 & \sigma_2^6 & \sigma_2^5 & \cdots & 1 \\ \vdots & \vdots & \vdots & \ddots & \vdots \\ \sigma_M^7 & \sigma_M^6 & \sigma_M^5 & \cdots & 1 \end{bmatrix}}_{\Phi} \cdot \underbrace{\begin{bmatrix} a_k^f \\ b_k^f \\ c_k^f \\ \vdots \\ f_k^f \end{bmatrix}}_{\theta_f} \tag{3.19}$$

The prediction error will be:

$$e = u - \hat{u} = u - \Phi\theta_f \tag{3.20}$$

The objective function to be minimized is:

$$J = \frac{1}{2} e^T e = \frac{1}{2}\left(u - \Phi\theta_f\right)^T \left(u - \Phi\theta_f\right) \tag{3.21}$$

The constraints are the first and second derivatives at the beginning and at the end of the polynomial.

$$\begin{aligned} u_s &= \frac{du}{ds} \\ u_{ss} &= \frac{du_s}{ds} = u_s \frac{du_s}{du} \end{aligned} \tag{3.22}$$

The boundary conditions at *u=0* and *u=1* can be represented in a system of linear equations.

$$\underbrace{\begin{bmatrix} 0 & 0 & 0 & 0 & 0 & 0 & 0 & 1 \\ 0 & 0 & 0 & 0 & 0 & 0 & 1 & 0 \\ 0 & 0 & 0 & 0 & 0 & 2 & 0 & 0 \\ 1 & 1 & 1 & 1 & 1 & 1 & 1 & 1 \\ 7 & 6 & 5 & 4 & 3 & 2 & 1 & 0 \\ 42 & 30 & 20 & 12 & 6 & 2 & 0 & 0 \end{bmatrix}}_{\Omega} \cdot \begin{bmatrix} a_7 \\ a_6 \\ a_5 \\ a_4 \\ a_3 \\ a_2 \\ a_1 \\ a_0 \end{bmatrix} = \underbrace{\begin{bmatrix} 0 \\ u_s(0)S \\ u_{ss}(0)S^2 \\ 1 \\ u_s(1)S \\ u_{ss}(1)S^2 \end{bmatrix}}_{\xi} \tag{3.23}$$

As a result, the optimization problem can be represented with the following objective function and constraints:

$$\begin{aligned} &\min \ \frac{1}{2}\left(u - \Phi\theta_f\right)^T \left(u - \Phi\theta_f\right) \\ &\text{subject to: } \Omega \cdot \theta_f = \xi \end{aligned} \tag{3.24}$$

This is a quadratic minimization problem with linear constraints, which can be solved with Lagrange Multipliers. The normalized coefficients of the feed correction polynomial are found from this linear equation system and they are de-normalized with the total displacement S.

3.6 Feedrate Optimization

In most of the FDM systems linear interpolation is used and the geometry of the toolpath is not considered while planning the trajectory. A constant feedrate is commanded for each section of the toolpath. However, the machine will slow down or make a full stop at the high curvatures and sharp corners even if the commanded feedrate is still the same. This is a natural behavior of the axes in order to decrease the contouring error. Every machine can handle this differently depending on the machine capabilities.

Minimum time feedrate optimization was proposed by Sencer [39] to minimize the cycle time by respecting the physical limitations of the drives. A B-Spline is fitted to the toolpath with a total length of $S_{\Sigma} = \sum_{k=1}^{N-1} S_k$. S_k is the path length between two consecutive toolpath points. Position commands are expressed as a function of path length s.

$$Q(s) = \begin{bmatrix} x(s) \\ y(s) \end{bmatrix} \tag{3.25}$$

The derivation of the feedrate ($\dot{Q}_{2x1}$), acceleration ($\ddot{Q}_{2x1}$) and jerk ($\dddot{Q}_{2x1}$) profiles are calculated by taking the first, second and third derivatives of the toolpath position Q(s) with respect to the path length s.

$$
\begin{aligned}
\dot{Q}(s) &= \frac{dQ}{dt} = \frac{dQ}{ds}\frac{ds}{dt} = Q_s(s)\cdot\dot{s}(s) \\
\ddot{Q}(s) &= \frac{d^2Q}{dt^2} = \frac{d^2Q}{ds^2}\left(\frac{ds}{dt}\right)^2 + \frac{dQ}{ds}\frac{d^2s}{dt^2} = Q_{ss}(s)\cdot\dot{s}^2(s) + Q_s(s)\cdot\ddot{s}(s) \\
\dddot{Q}(s) &= \frac{d^3Q}{dt^3} = \frac{d^3Q}{ds^3}\left(\frac{ds}{dt}\right)^3 + 3\frac{d^2Q}{ds^2}\frac{ds}{dt}\frac{d^2s}{dt^2} + \frac{dQ}{ds}\frac{d^3s}{dt^3} \\
&= Q_{sss}(s)\cdot\dot{s}^3(s) + 3Q_{ss}(s)\cdot\dot{s}(s)\cdot\ddot{s}(s) + Q_s(s)\cdot\dddot{s}(s)
\end{aligned}
\tag{3.26}
$$

where $\dot{s}(s) = \frac{ds}{dt}, \ddot{s}(s) = \frac{d^2s}{dt^2}$ and $\dddot{s}(s) = \frac{d^3s}{dt^3}$ are the tangential feed, acceleration and jerk along the path *s*. A cubic B-Spline defined with third order blending functions $(N_{i,3})$ is fitted to the tangential feeds along the path:

$$
\dot{s}(v) = N_{0,3}(v)\cdot f_0 + N_{1,3}(v)\cdot f_1 + \ldots + N_{n-1,3}(v)\cdot f_{n-1} = \sum_{i=0}^{n-1} N_{i,3}(v)\cdot f_i \tag{3.27}
$$

where f_i are the feedrate control points along the entire toolpath and their initial value is as half the desired tangential feed. The first and second derivatives (the acceleration and jerk) of the B-Spline in Eq. (3.27) are:

$$
\begin{aligned}
\ddot{s}(v) &= \frac{d\dot{s}(v)}{dv} = \frac{dN_{0,3}(v)}{dv} f_0 + \ldots + \frac{dN_{n-1,3}(v)}{dv} f_{n-1} \\
\dddot{s}(v) &= \frac{d^2\dot{s}(v)}{dv^2} = \frac{d^2N_{0,3}(v)}{dv^2} f_0 + \ldots + \frac{d^2N_{n-1,3}(v)}{dv^2} f_{n-1}
\end{aligned}
\tag{3.28}
$$

where $v \cong s\cdot(1/S_\Sigma)$ and S_Σ is the total length of the toolpath. Since v is linearly related to s:

$$\begin{aligned}\dot{s}(v) &= \dot{s}(s/S_\Sigma) = \dot{s}(s)\\ \ddot{s}(v) &= \ddot{s}(s/S_\Sigma) = \ddot{s}(s)\\ \dddot{s}(v) &= \dddot{s}(s/S_\Sigma) = \dddot{s}(s)\end{aligned} \tag{3.29}$$

As a result, feed ($\dot{s}(s)$), acceleration ($\ddot{s}(s)$) and jerk ($\dddot{s}(s)$) are defined as functions of displacement (s) along the splined path. Additional details are given in [40].

The objective is to minimize the printing time without exceeding the feed imposed by the extrusion rate and the velocity, acceleration and jerk limits of *x* and *y* drives of the machine. The objective function is formulated to have a minimum travel time (T_Σ) across the whole tool path:

$$\min(T_\Sigma) = \min \int_0^{S_\Sigma} dt \tag{3.30}$$

where the differential travel time per segment of the path is $dt = ds/\dot{s}(s)$ and the objective function becomes:

$$\min \int_0^{S_\Sigma} \frac{ds}{\dot{s}(s)} \text{ subject to } \{\dot{s}, \ddot{s}, \dddot{s}\} \le \{\text{Axis Limits}\} \tag{3.31}$$

The kinematic (velocity, acceleration and jerk) constraints are defined without exceeding the axis limitations. The axes velocity, acceleration and jerks in Eq. (3.26) are normalized with the axes limits as follows:

$$
\begin{aligned}
&-\begin{bmatrix}1\\1\end{bmatrix} \le \underbrace{\begin{bmatrix} x_s(s)/v_{x,\max} \\ y_s(s)/v_{y,\max}\end{bmatrix}}_{Q_s^v} \dot{s}(s) \le \begin{bmatrix}1\\1\end{bmatrix} \\
&-\begin{bmatrix}1\\1\end{bmatrix} \le \underbrace{\begin{bmatrix} x_{ss}(s)/a_{x,\max} \\ y_{ss}(s)/a_{y,\max}\end{bmatrix}}_{Q_{ss}^a} \dot{s}(s)^2 + \underbrace{\begin{bmatrix} x_s(s)/a_{x,\max} \\ y_s(s)/a_{y,\max}\end{bmatrix}}_{Q_s^a} \ddot{s}(s) \le \begin{bmatrix}1\\1\end{bmatrix} \\
&-\begin{bmatrix}1\\1\end{bmatrix} \le \underbrace{\begin{bmatrix} x_{sss}(s)/J_{x,\max} \\ y_{sss}(s)/J_{y,\max}\end{bmatrix}}_{Q_{sss}^j} \dot{s}^3(s) + 3\underbrace{\begin{bmatrix} x_{ss}(s)/J_{x,\max} \\ y_{ss}(s)/J_{y,\max}\end{bmatrix}}_{Q_{ss}^j} \dot{s}(s)\ddot{s}(s) + \underbrace{\begin{bmatrix} x_s(s)/J_{x,\max} \\ y_s(s)/J_{y,\max}\end{bmatrix}}_{Q_s^j} \dddot{s}(s) \le \begin{bmatrix}1\\1\end{bmatrix}
\end{aligned}
$$

(3.32)

The control points of the feed profile ($\dot{s}(s)$) are selected with MATLAB's ™ [41] non-linear convex optimization engine to minimize the objective function defined by Eq. (3.30) while respecting the constraints defined in Eq. (3.32). The velocity, acceleration and jerk of the drives obey their physical limits while minimizing the travel time. Additional details of the optimization algorithm are given by Sencer et al. [39].

The feed profile is defined as a function of path displacement ($\dot{s}(s)$) as the result of the optimization algorithm and it is used to generate the position commands at the sampling frequency of the servo loop. The toolpath starts at $s = 0$ and Taylor Expansion is used to generate the displacement commands at each sample time, where the toolpath starts with $s = 0$ at the initial time step ($k = 0$) as $s[k] = s[0] = 0$.

$$
s[k+1] = s[k] + T_s \dot{s}(s) + \frac{T_s^{\,2}}{2} \ddot{s}(s) \tag{3.33}
$$

where T_s is the sample time of the servo loop and the feed and acceleration profiles $\dot{s}(s)$ and $\ddot{s}(s)$ are evaluated at the displacement at the current time step $s[k]$ which is defined in Eqs. (3.26), (3.27) and (3.28). From the displacement commands $s[k]$, position commands can be generated by substituting $s[k]$ into Eq. (3.12) then into Eq. (3.3) as follows

$$P(u(s[k])) = \begin{Bmatrix} x(k) \\ y(k) \end{Bmatrix} \tag{3.34}$$

Since $P(u)$ is jerk continuous, $u(s)$ is jerk continuous, and $s[k]$ is defined by the jerk continuous feed profile $\dot{s}(s)$ then the position commands $x[k]$ and $y[k]$ are also jerk continuous.

In this optimization problem, the resulting tangential velocity is used as the extrusion rate profile by simply scaling it with a constant parameter. The limiting factor in this problem is how fast the extruder can feed the material into the nozzle. The torque limit of the stepper motor of the extruder, the diameter of the nozzle and filament, the printing temperature and the material properties need to be considered determine the upper limit of the extrusion rate.

3.7 Synchronizing Material Extrusion Rate with Tangential Feedrate

A linear relationship is defined between tangential path velocity and extrusion rate. It is assumed that there is no material loss through the entire extruder, so that the whole amount of fed material comes out from the nozzle with a different diameter and length. It means that the volumetric flow rate before and after filament deformation remains the same.

$$\dot{V}_i = \dot{V}_f \tag{3.35}$$

The volumetric flow rate can be represented as a function of linear velocity and the cross-sectional area of the filament before and after it's extruded through the nozzle.

$$\begin{aligned} A_i \cdot V_i &= A_f \cdot V_f \\ \frac{\pi d_i^2}{4} \cdot V_i &= \frac{\pi d_f^2}{4} \cdot V_f \end{aligned} \tag{3.36}$$

where A_i and A_f are the initial and final cross-sectional areas, and d_i and d_f are the initial and final diameters of the filament, respectively. So there is a linear relationship between the initial and final velocities of the filament and this relationship is defined by the ratio of initial and final diameters of the filament. It is assumed that the final diameter of the filament is the same with the nozzle diameter.

In order to have a continuous flow and a homogeneous deposition profile, the extrusion rate of the filament at the exit of the nozzle should be linearly proportional to the tangential feedrate of the printing table assuming that there is no loss of material in the nozzle. However, the extruder may still need a calibration, which is done with a fixed temperature at 210 ^{o}C.

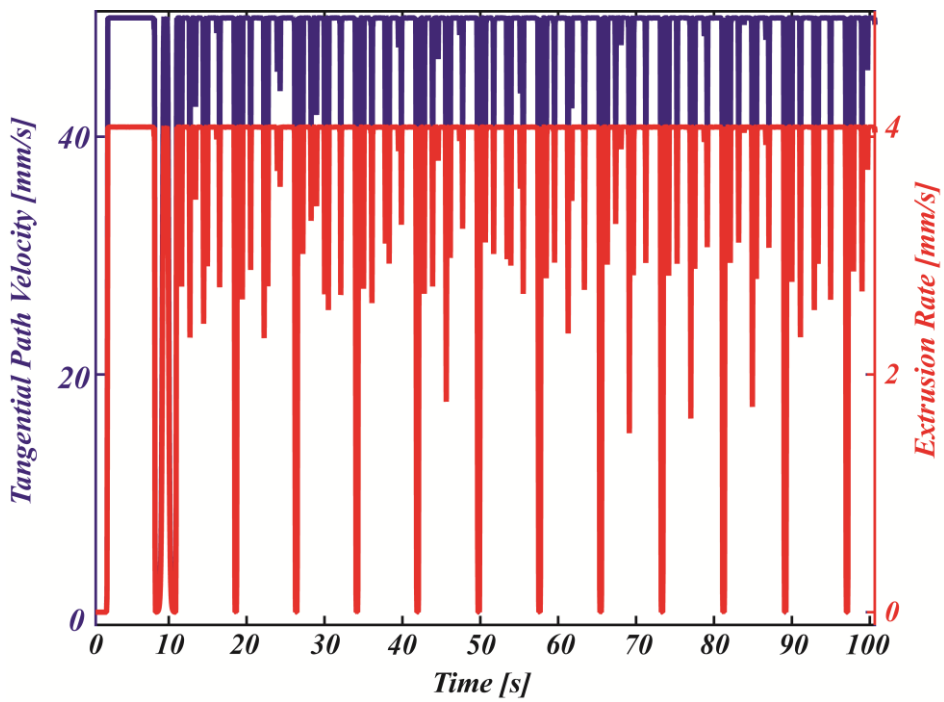

Figure 3.2 Synchronized Tangential Path Velocity and Extrusion Rate

The relationship between the tangential feedrate and extrusion rate is defined as:

$$V_f = \mu \cdot V_t \tag{3.37}$$

where V_t is the tangential federate along the path. If the constant (μ) is increased or decreased, the change in deposition profile will be visible. Increasing the ratio will result in a smaller deposition cross section area (with a smaller diameter) and may result in some discontinuities in the profile. With a lower ratio, a bigger deposition cross section area (with a bigger diameter) will be printed.

3.8 Conclusion

It is necessary to synchronize the extrusion rate with the feedrate in order to have a homogeneous and continuous deposition profile by printing 3D objects with complex geometries. The commercial CAM software for FDM processes provides constant extrusion rate, which can be changed only from one layer to the other one. For simple geometries, a constant extrusion rate can be preferred because it is only one operation to get the G-codes, it's not time consuming and also saves a lot from the computational time. It can promise a decent surface finish and deposition profile. On the other hand, the method proposed in this chapter can handle complex geometries without making a concession from a good surface finish and deposition profile. Synchronizing the extrusion rate with the feedrate makes the toolpath smoother in order to minimize the fluctuations in the trajectory profiles. It generates the trajectory profiles with considering the geometry of the toolpath to capture the feedrate fluctuations through the process. In comparison to the commercial method, it requires more computation time but it enhances the surface finish and deposition profile for parts having complex geometries.

Chapter 4: Adaptive Temperature Control of FDM Heater System

4.1 Overview

Synchronizing the extrusion rate with the tangential path velocity brings fluctuations in the extrusion rate profile. As a result, the amount of material deposited per unit time changes, where the heat transferred to the material is still constant. A constant heat rate through the whole process, while the extrusion rate changes, may cause over- or under-heated filament sections. If a section of filament is under-heated, more force will be needed in order to extrude the filament through the nozzle because it's less viscous. If it's over-heated, the material can degrade and its physical and chemical properties can change, and the printed shape control becomes difficult due to spread of liquid material. It is desired to maintain a constant temperature at the filament as the material flow rate changes in the heated nozzle of the extruder.

The heat model should consider how fast the material is deposited and how it's changing. Although the response of the heating system is slower than the extruder system in general because of the system's physical limitations, it should be designed as a function of the extrusion rate. The temperature response can be seen with changing extrusion rate in Figure 4.1.

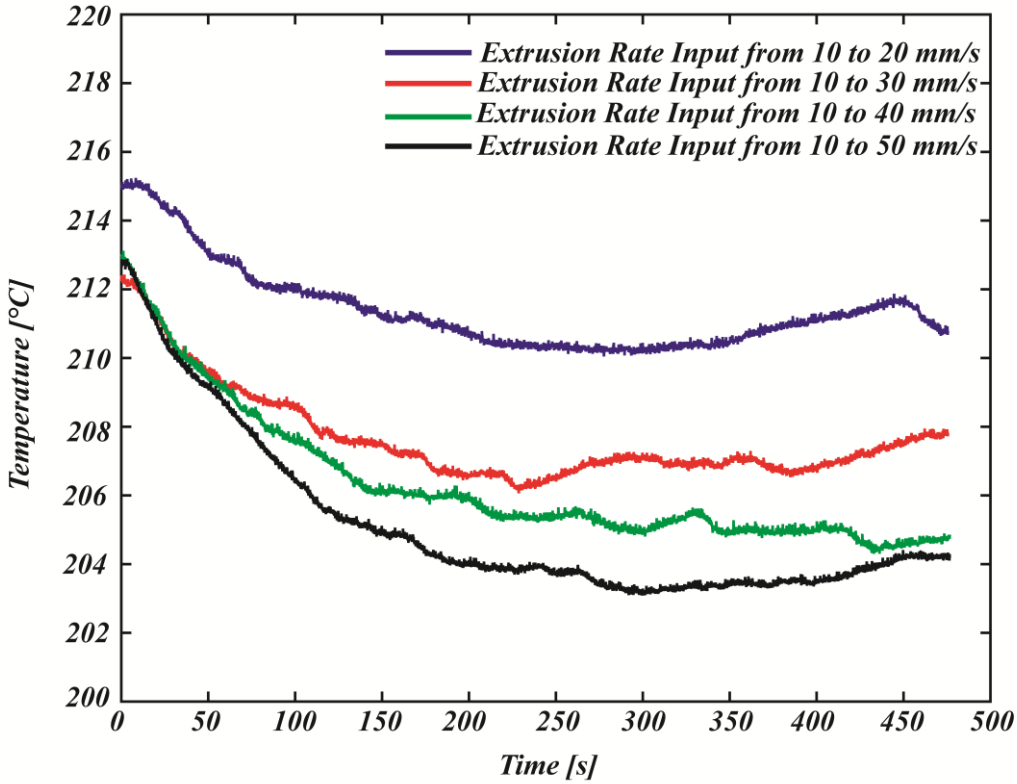

Figure 4.1 The Change in Temperature with Extrusion Rate

FDM systems usually have a built-in PID (proportional, integrator, derivative) controller or the extruder manufacturers recommend to put a PID controller with the given proportional, integrator and derivative gains (K_p, K_i, K_d), which doesn't involve modeling of the system and designing the controller. Moreover, the controller tries to keep the temperature constant without considering the changes in the extrusion rate profile. If the extrusion rate increases and more material is deposited at a certain amount of time, it will take more heat from the environment and the energy loss becomes higher. However, the temperature responds to this change after some time delay and the power supplied to the heater will be lower with the effect of PID controller.

When the heater provides more energy to the system, it is possible to have a low extrusion rate and excessive heat will be transferred to the material. It is important to know the extrusion rate commands before the process and manipulate the heating system according to the extrusion rate.

In this chapter the heater of the FDM system is modeled and a controller is designed as a function of extrusion rate commands in order to keep the temperature constant.

4.2 Heating System of FDM

The heating system consist of an aluminum block, a finned cylinder and a fan. The aluminum block is the part where the heater coil and the thermistor are placed and the filament is fed through. The finned cylinder is on top of the aluminum block and it is surrounding the filament. The fan is located across the finned cylinder. It is important to have the fan working all the time while the heater is on. When the fan does not work, the heat will diffuse through the filament from the heater to upwards, where the filament needs to stay solid. After the filament gets hot enough, the material softens and because of the feeding force provided from the gears the filament buckles. It results in clogging of the nozzle. It's important to have the fan working all the time through the printing process. The finned cylinder around the filament increases the surface area, where the heat transfer occurs. The heating model in this thesis considers the heat loss to the environment and through the material flow.

The heater has a 12 Volt amplifier with 60 Watt power capacity at the coiled resistor. The resistor is placed near to the cylindrical chamber, where the filament is fed. The thermistor is

located between the heater resistor and the hole for the filament. It measures the temperature at each millisecond.

The aluminum block has holes for homogeneous heat distribution through the whole aluminum block. As the filament is heated from only one side, the temperature distribution becomes more important and a solid aluminum block may bring some temperature differences between two sides of the filament.

The resistance of the heater resistor is measured at different temperatures within the printing temperature range in order to see if there is an effect of temperature on the resistance. There is only 4% change on the resistance value in the printing temperature range, which is neglected and the resistor is assumed to have a constant value of 2.4 ohms.

4.3 Transfer Function of the FDM Heater

The dynamic model of the heater is constructed by considering only the conduction at the aluminum heating block, where the transfer of energy occurs between two objects (aluminum block and filament) which are in contact. The finned cylinder and the fan cause heat losses from the top of the aluminum block as the fan works with 100% capacity throughout the printing process. The effect of finned cylinder, the fan and the other energy loses to the environment reduce the efficiency coefficient, which is identified experimentally. Within a given threshold the power source goes on and off when the response exceeds the upper and lower power limits of the heater. The disadvantage of this controller is that it always operates at the saturation limits. The

efficiency of the heater is defined by the ratio of the time when the power source is on over the total time of the printing process.

The solid filament at room temperature is fed through the cylindrical extrusion chamber where it is heated and deposited to the table through conical injector nozzle. The temperature of the material is controlled by manipulating current flow to the resistance circuit of the heater. The net heat (E_{stored}) can be defined by using the first law of thermodynamics:

$$E_{stored} = \eta_{heff} E_{in} - E_{loss} \tag{4.1}$$

where E_{in} is the heat supplied from the heating coil with an efficiency coefficient η_{heff} and E_{loss} is the heat losses through the material flow. By considering the material properties, mass flow rate and temperature gradient, the heat balance becomes:

$$\underbrace{m_{Al} c_{Al} \frac{\partial T_A(t)}{\partial t}}_{E_{stored}} = \eta_{heff} \underbrace{\frac{T_R(t) - T_A(t)}{L_{eq}} A_{eq} k_{Al}}_{E_{in}} - \underbrace{\dot{m} c_{PLA} \left(T_A(t) - T_i \right)}_{E_{loss}} \tag{4.2}$$

where $\dot{m}[kg/s]$ is the mass flow rate in the heating zone, c_{PLA} is the specific heat capacity of the filament material, respectively; T_i is the initial temperature of the filament as it enters the heating chamber; $T_R(t)$ and $T_A(t)$ are the reference and measured printing temperatures of the filament. The properties of the aluminum heater block are represented by the mass (m_{Al}), the specific heat capacity (c_{Al}) and the thermal conductivity (k_{Al}), which are known. The complex

geometry of the heater is approximated by the equivalent length (L_{eq}) and area (A_{eq}) between the heating coil and heated filament area, respectively. The heat transfer equilibrium can be parameterized as:

$$\frac{\partial T_A(t)}{\partial t}+\left[\frac{\eta_{heff}}{\left(\frac{L_{eq}}{A_{eq}k_{Al}}\right)m_{Al}c_{Al}}+\frac{\dot{E}(t)A_{PLA}\rho_{PLA}c_{PLA}}{m_{Al}c_{Al}}\right]T_A(t)=\frac{\eta_{heff}}{\left(\frac{L_{eq}}{A_{eq}k_{Al}}\right)m_{Al}c_{Al}}T_R(t)+\frac{\dot{E}(t)A_{PLA}\rho_{PLA}c_{PLA}}{m_{Al}c_{Al}}T_i$$

(4.3)

where the known material properties of the filament are the density ($\rho_{PLA}\left[kg/m^3\right]$), specific heat capacity ($c_{PLA}\left[J/kg^oC\right]$) and the cross-section area $A_{PLA}\left[m^2\right]$. The extrusion rate $\dot{E}\left[mm/s\right]$ is time varying and it is changing the dynamics of the system at each time step.

The reference temperature is defined by the heat provided from the heater. Heating power can be represented with the square of the supplied current ($I^2(t)$) to the heating coil with the resistance of R_h .

$$T_R(t)=\frac{R_h}{m_h c_h}u(t)\leftarrow u(t)=I^2(t) \tag{4.4}$$

where m_h, c_h are the mass and specific heat capacity of the heater coil. When the constants of material and geometric properties of the heater block and filament are lumped together the model in Eq. (4.3) becomes:

$$\frac{\partial T_A(t)}{\partial t} + \left[\alpha_1 + \alpha_2 \dot{E}(t)\right] T_A(t) = \beta u(t) + \alpha_2 \dot{E}(t) T_i \tag{4.5}$$

where the time invariant parameters ($\alpha_1, \alpha_2, \beta$) are identified from the known properties of the system and identification experiments:

$$\alpha_1 = \frac{\eta_{heff}}{\left(\frac{L_{eq}}{A_{eq} k_{Al}}\right) m_{Al} c_{Al}} \quad ; \quad \alpha_2 = \frac{A_{PLA} \rho_{PLA} c_{PLA}}{m_{Al} c_{Al}} \quad ; \quad \beta = \alpha_1 \frac{R_h}{m_h c_h} \tag{4.6}$$

The initial temperature (T_i) can be dropped from the transfer function because it is just an initial condition and doesn't affect the system response. By taking the Laplace transform, the transfer function of the heating system is expressed as:

$$G(s) = \frac{T_A(s)}{u(s)} = \frac{\beta}{s + p} \quad \leftarrow p = \alpha_1 + \alpha_2 \dot{E}(t) \tag{4.7}$$

Where the pole (p) of the system depends on the time varying extrusion rate $\left(\dot{E}(t)\right)$. When the extrusion rate drops almost to zero $\left(\dot{E}(t) \approx 0\right)$ at sharp corners, the heat is absorbed only by the aluminum heater block ($E_{stored} = \eta_{heff} E_{in}$) which reduces the pole from $p = \alpha_1 + \alpha_2 \dot{E}(t) \rightarrow p = \alpha_1$ during the servo control of the temperature.

The ratio of L_{eq} / A_{eq} is identified experimentally, where a current step input is given and temperature is measured without extruding the material. As it represents a geometrical property,

it is constant for every case. The ratio is calculated from the time constant of the system. The transfer function of the system without extrusion is:

$$\frac{T_A(s)}{T_R(s)} = \frac{\eta_{heff}}{\frac{L_{eq}}{A_{eq}k_{Al}} m_{Al}c_{Al}s + \eta_{heff}} \tag{4.8}$$

The time constant of a first order system is the time passed from the beginning of the experiment until the response reaches the 63.2% of the steady state value shown in Figure 4.2.

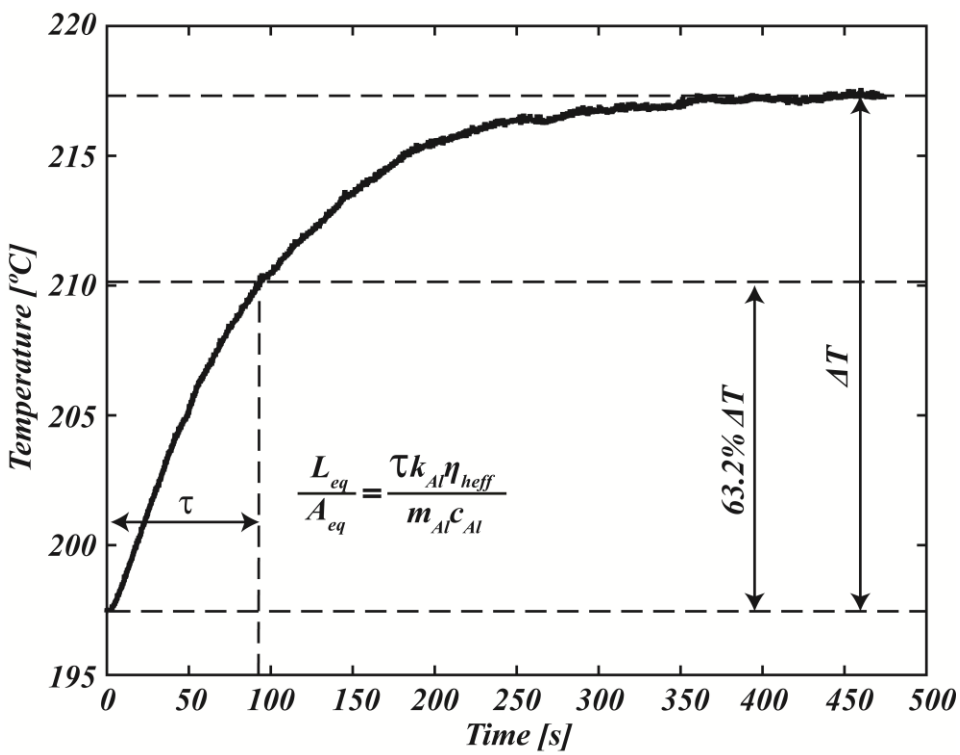

Figure 4.2 Experimental Identification

4.4 Controller Design

In order to have a stable system for all extrusion rate values within the feasibility range, a pole placement (PP) controller is designed in discrete time domain. In this controller, the design requirements are defined and the stable poles of the closed loop transfer function are assigned according to the design requirements.

PP controller has three polynomials with different degrees: $S\left(z^{-1}\right)$, $T\left(z^{-1}\right)$ and $R\left(z^{-1}\right)$, which represent feedback, feed-forward and error regulators, respectively.

$$\begin{aligned} T\left(z^{-1}\right) &= t_0 \\ S\left(z^{-1}\right) &= s_0 + s_1 z^{-1} + s_2 z^{-2} + \ldots + s_f z^{-f} \\ R\left(z^{-1}\right) &= 1 + r_1 z^{-1} + r_2 z^{-2} + \ldots + r_p z^{-p} \end{aligned} \tag{4.9}$$

As the plant changes continuously through the entire process, the controller parameters are adapted to the varying extrusion rate as follows.

The zero order hold equivalent of the heater (Eq.(4.7)) at δt discrete time intervals is obtained as:

$$\begin{gathered} G(z) = \frac{T_A(n)}{u(n)} = z^{-1}(1 - z^{-1}) Z\left[\frac{G(s)}{s}\right] = \frac{b(n) z^{-2}}{1 + a(n) z^{-1}} \\ b(n) = 1 - e^{-p(n)\cdot\delta t}\ ,\ a(n) = -e^{-p(n)\cdot\delta t} \leftarrow p(n) = \alpha_1 + \alpha_2 \dot{E}(t) \end{gathered} \tag{4.10}$$

where n is the sampling number, z^{-1} is the communication delay in the computer.

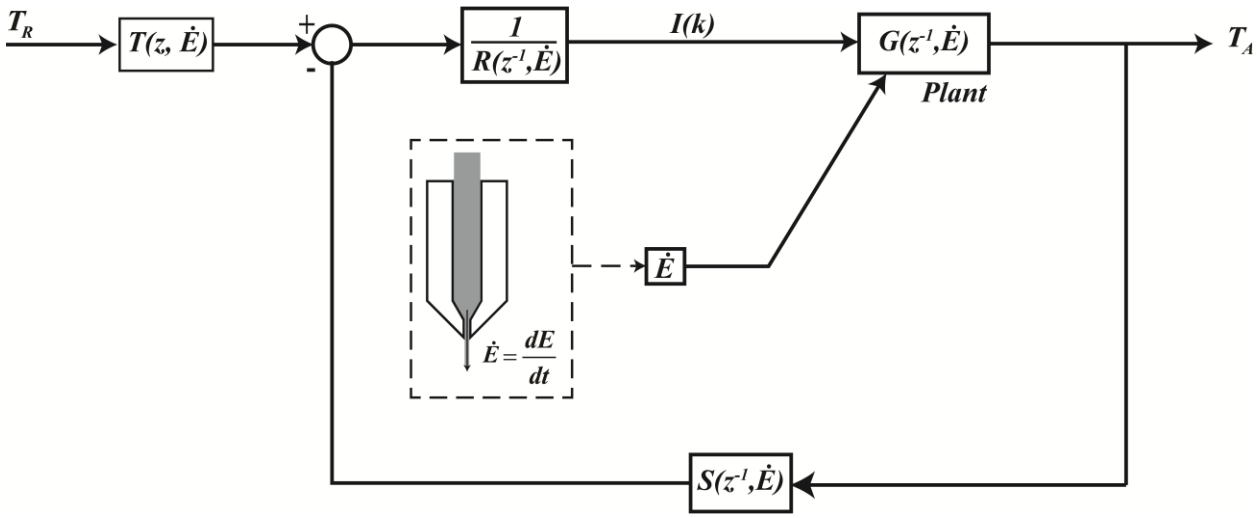

Figure 4.3 Heating System of FDM Machine

An adaptive pole placement controller is designed to keep the temperature of the extruded filament by manipulating the current supplied to the heater's coil as shown in Figure **4.3**. The desired characteristic equation is calculated according to the design requirements of damping ratio $\zeta = 0.8$ and natural frequency $\omega_n = 0.01$ Hz:

$$s^2 + 2\varsigma\omega_n s + \omega_n{}^2 = (s-p)(s-p^*) \leftarrow p, p^* = -\varsigma\omega_n \pm j\omega_n\sqrt{1-\varsigma^2} \tag{4.11}$$

The discrete equivalent ($z_1 = e^{pT}; z_2 = e^{p^*T}$) of the poles of the desired characteristic equation becomes:

$$\begin{aligned} A_m(z) &= (z^{-1} - z_1)(z^{-1} - z_2) = 1 + m_1 z^{-1} + m_2 z^{-2} \\ m_1 &= -2e^{-\varsigma\omega_n T}\cos\left(\omega_n\sqrt{1-\varsigma^2}T\right); m_2 = e^{-2\varsigma\omega_n T} \end{aligned} \tag{4.12}$$

The orders of the controller polynomials are determined according to the order of the nominator and denominator of the transfer function. The controller parameters are evaluated as follows:

$$
\begin{aligned}
S(z^{-1}) &= s_0 = -\frac{b(n)\cdot m_2}{a(n)\cdot(a_1 - m_1) + m_2} \\
R(z^{-1}) &= 1 + r_1 z^{-1} \leftarrow r_1 = \frac{m_2}{a(n)} \\
T &= t_0 = \frac{1 + m_1 + m_2}{b(n)}
\end{aligned}
\tag{4.13}
$$

The current control command ($u(n) = I^2(n)$) at each sampling interval n becomes:

$$
u(n) = -r_1 u(n-1) + t_0 T_R(n) - s_0 T_A(n) \tag{4.14}
$$

where the control parameters r_1, s_0, t_0 are adaptively adjusted at each sampling interval from Eq.(4.13) as the extrusion rate changes.

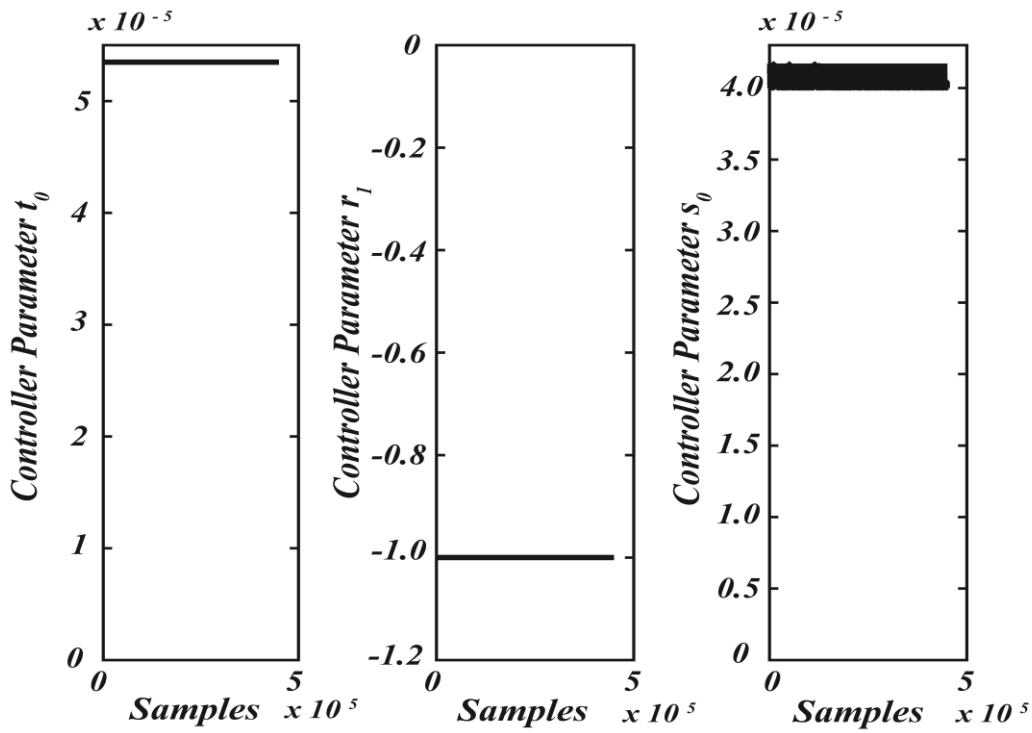

Figure 4.4 Controller Parameters

The thermal mass of the aluminum block is much higher than the thermal mass of the filament heated in the nozzle ($m_{Al}c_{Al} \gg m_{PLA}c_{PLA}$), the parameter changes are low in practice for this particular application, which can be seen in Figure 4.4. A sample experimental result is shown in Figure 4.5, where the extrusion rate varies.

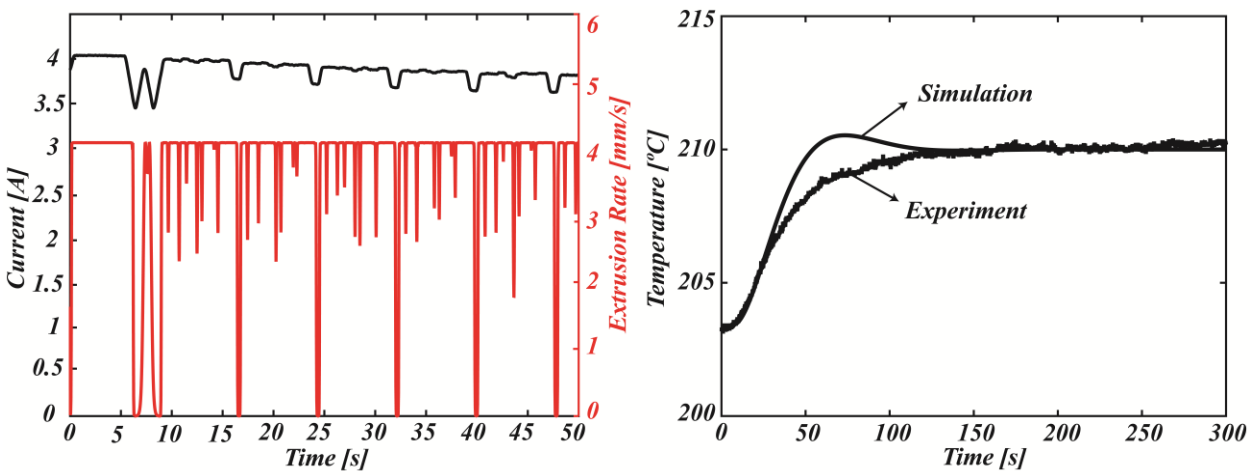

Figure 4.5 Adaptive control of temperature as the extrusion rate changes along the tool path. a) Current command history b) Transient change of the temperature before the extrusion and steady state temperature control after the extrusion starts.

The same experiment is also done with constant extrusion rate, where there is no fluctuation in the current commands.

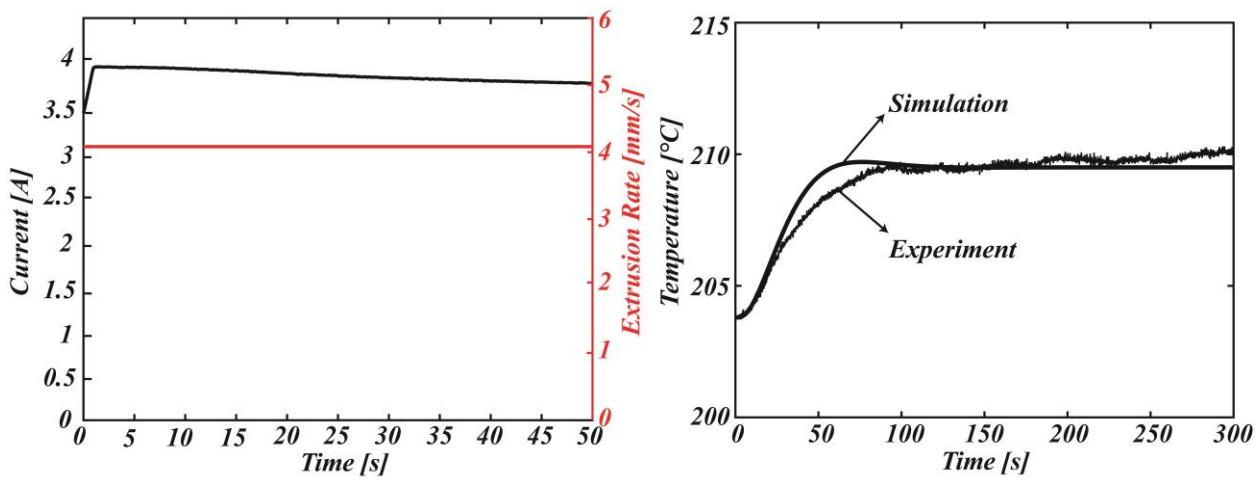

Figure 4.6 Adaptive control of temperature as the extrusion rate remains the same along the tool path. a) Current command history b) Transient change of the temperature before the extrusion and steady state temperature control

There is a good match between simulation and experiment results at the steady state region. There is a difference at the transient portion of the simulation because the actual system has a bigger damping ratio than the temperature model.

4.5 Conclusion

In this chapter the heater of the FDM system is modeled by considering the conduction at the aluminum heater block. The model includes the thermal, material and geometric properties of the components such as filament, heater block and heater coil, which are known. The ratio of the equivalent length (L_{eq}) and area (A_{eq}) between the heating coil and heated filament area, is identified experimentally. The model is proven experimentally. An adaptive pole placement

controller is designed in order to keep the temperature constant through the entire printing process. Although the extrusion rate is time varying, the temperature is kept constant during the printing process.

Chapter 5: Printing Simulations and Experiments

5.1 Overview

In this chapter, the experimental setup, the validation of the synchronization of the extrusion rate with the tangential path velocity of the printing table and the temperature model of the FDM's heating system are presented. The advantages and disadvantages of the models proposed in this thesis are discussed and compared against the current FDM technology.

In order to validate the extrusion rate profile synchronized with the tangential path velocity, the same geometry is printed with constant and velocity dependent extrusion profiles. The temperature through the process is recorded with a thermistor and compared against the simulation results.

5.2 Experimental Setup

An in-house built 9-axis CNC micro metal cutting machine retrofitted with a filament injector is used in the experiments shown in Figure 5.1. The machine and the process are controlled by the modular, open architecture CNC [42], which is based on dSpace and real time digital signal processing system. As the FDM operation needs only 3 axes (x, y, z), the rotary

table with six degrees of freedom is kept stationary. The printing table is located on the x and y drives, and the extruder head is positioned on the z drive of the machine.

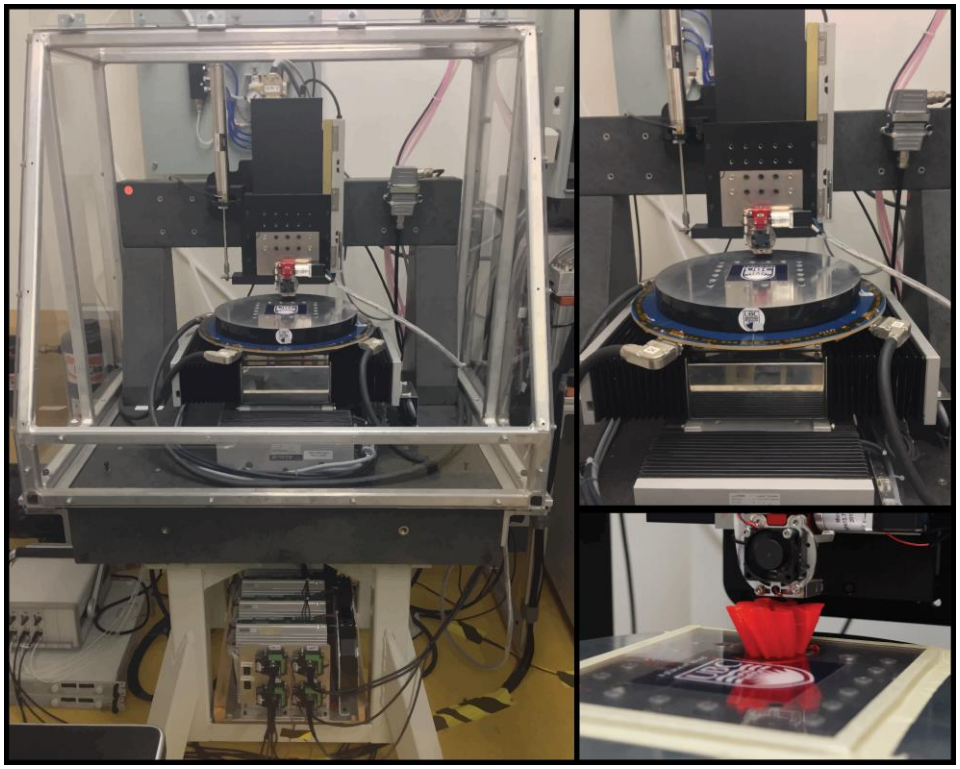

Figure 5.1 Experimental Setup

The position commands are given as an input to the system and through the dSPACE, the control commands are sent to the linear drives at each sampling time. The feedback comes from the encoder for each linear drive. The trajectory is planned before the operation and time sampled position commands are stored in a file and fed to the system through the dSPACE. In addition to the time sampled position data, the extrusion rate commands are also given in the input commands to the machine. The extrusion rate commands are used to drive the stepper

motor to feed the material into the extruder, and to calculate the controller parameters for the heating system. Calculating every controller parameter before the process and giving them as an input to the system are not preferred because this would bring three additional input to the system, which makes the communication protocol more complex.

The extruder unit includes the stepper motor for the feeding system, which consists of two gears. The filament material first goes through the heater, where the filament is heated up to its melting point. The heated filament is deposited through the nozzle. As the feeding system is an open loop system without a feedback of true extrusion rate, it is essential to calibrate the extruder for a certain printing temperature, filament material and nozzle diameter. The excessive heat is dissipated with the help of the finned cylinder and the fan, which is kept constant through the entire process.

A Polylactic Acid (PLA) filament with a diameter of 1.75 mm is used in the experiments. The nozzle, where the filament is extruded through, has a diameter of 0.5 mm. The printing temperature is set to 210°C.

3D parts are designed with sharp corners and high curvatures (Figure 5.3) and they are created in Siemens NX CAD software. Slic3r is used to slice the part for tool-path generation. The process properties are given as a user input to the software. Since only position commands are taken from the generated machine code (e.g. G-Code), only the required layer height is defined as a process parameter. The layer height is set to 0.25 mm for the first layer and 0.35 mm for the remaining layers. Path smoothing algorithm is applied to the position commands and a

fifth order B-Spline is fit to the tool-path points (Figure 5.2). The feed correction polynomial is defined to identify the relationship between the path segment lengths and geometric spline parameter u $\left(u = u\left(s\right)\right)$.

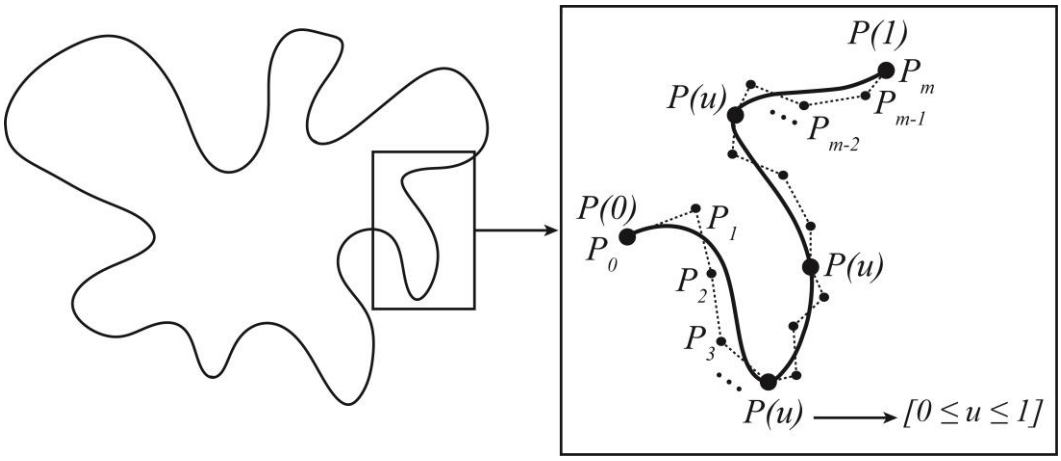

Figure 5.2 Spline Fitting on Toolpath Points

Feedrate optimization algorithm is used to generate the time sampled position data and the trajectory profiles. The extrusion rate commands are synchronized with the tangential path velocity with a linear relationship.

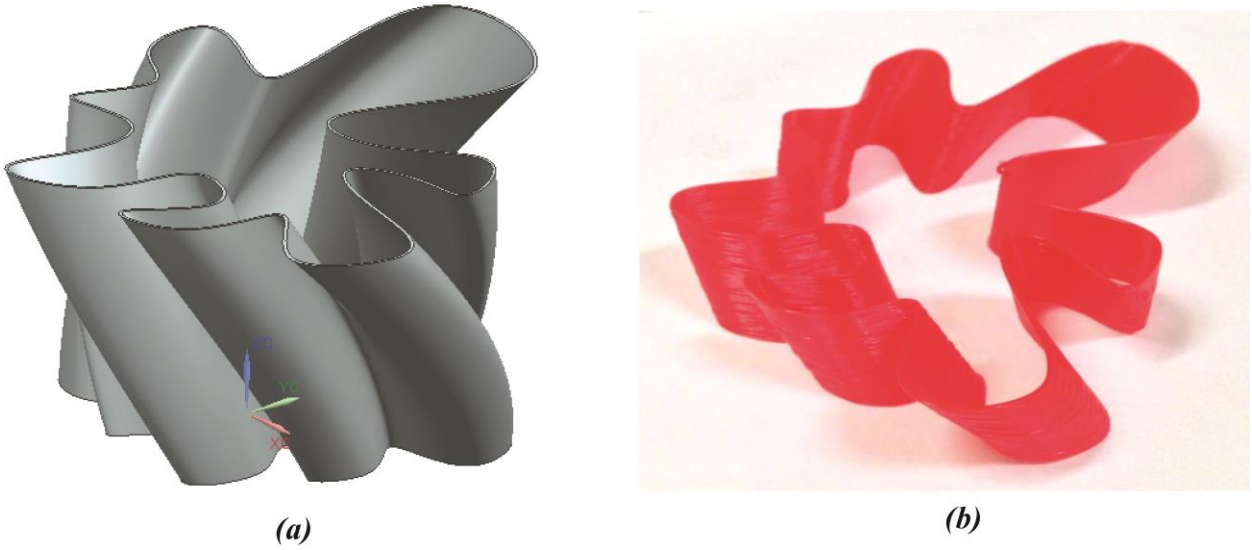

Figure 5.3 3D Parts Printed in the Experiments (3D CAD Part (a) and 3D Printed Part (b))

5.3 Experimental Results for the Extrusion Rate Profile

The 3D part is first printed with the extrusion rate synchronized with the tangential path velocity. The same part with the same toolpath is printed with constant extrusion rate as a reference of current technology for FDM operations. The parts are compared against each other to show the effect of synchronization.

A linear relationship is defined in Chapter 3 in order to have a homogeneously distributed deposition profile and to keep the width of the layer constant along the toolpath. The width of the printed filament depends on the extrusion rate and the table speed. The unsynchronized motion of extrusion rate and table speed will result in deposition profile sections with varying width. This can be seen in the Figure 5.4a, where the extrusion rate is not synchronized and kept

constant through the process. The excessive material accumulation can be seen at the sharp corner in Figure 5.4a, where the printing table slows down in order to decrease the tracking error. The extruder keeps depositing material at the same rate, which causes inhomogeneous deposition profile and a rough surface finish at this point of the part. The part printed with synchronized extrusion rate (Figure 5.4b) has a better surface finish and homogeneously distributed deposition profile in comparison to the part printed with constant extrusion rate.

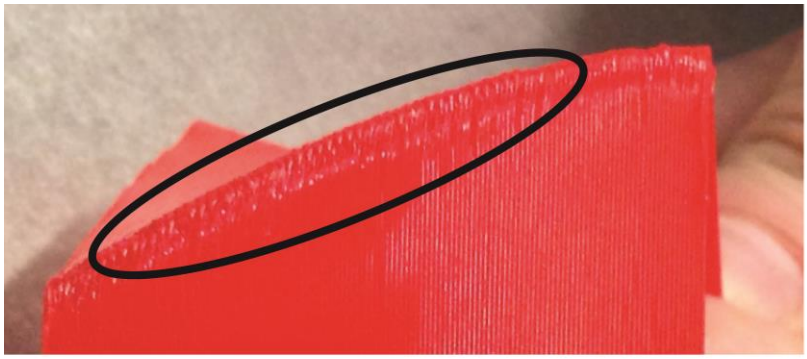

a)

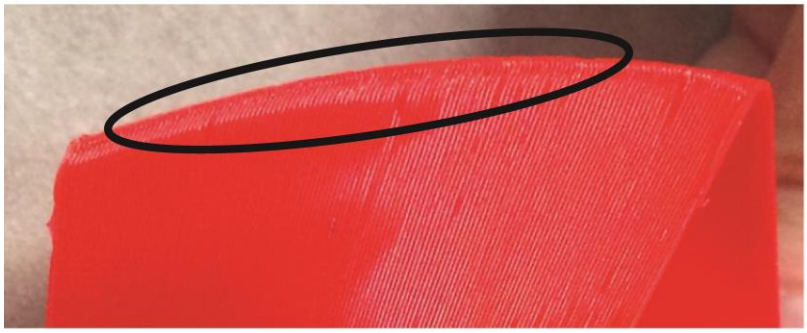

b)

Figure 5.4 Deposition Profile Comparison between Constant Extrusion Rate (a) and Synchronized Extrusion Rate (b)

The synchronization algorithm gives a smoother surface finish as expected. Overall it requires more time to generate the extrusion rate profile. However, the synchronization becomes more necessary, when the part geometry gets more complex.

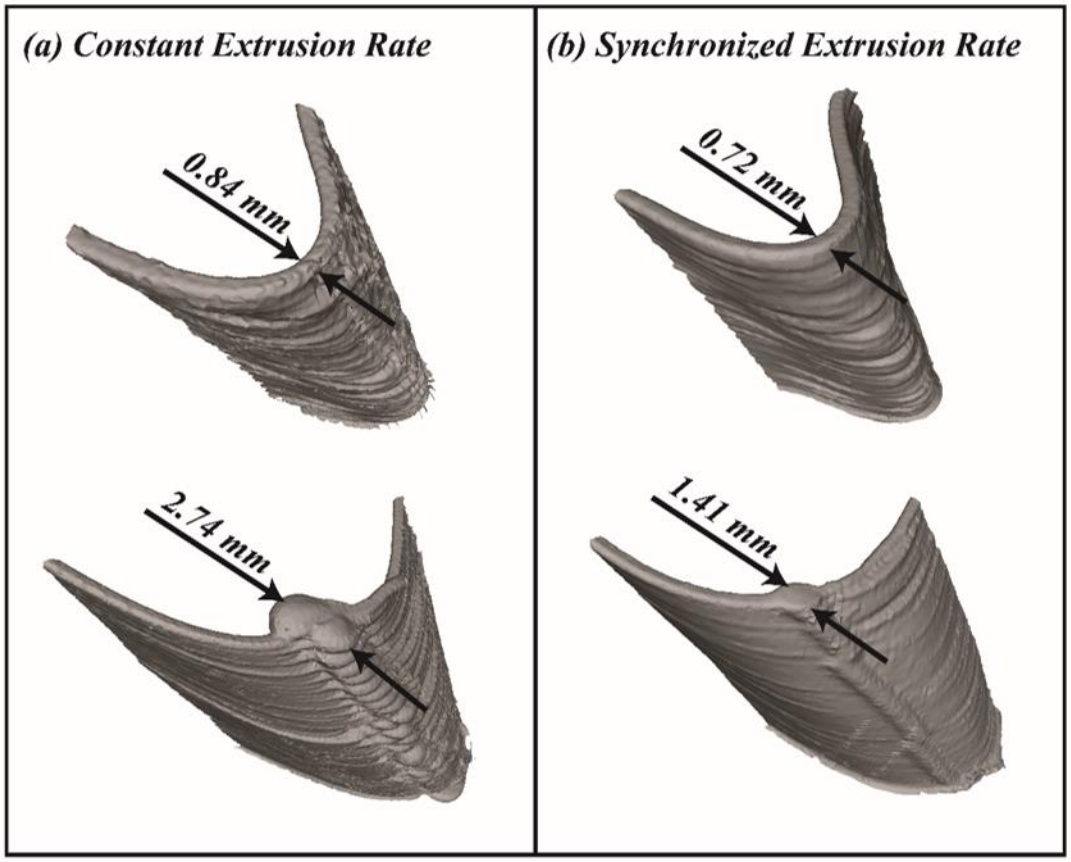

Figure 5.5 3D Laser Scan of Two Curves of the Part with constant (a) and synchronized (b) extrusion rates

The parts printed with constant extrusion rate and synchronized extrusion rate are scanned with a 3D laser scanner in order to quantify the difference between constant extrusion rate and synchronized extrusion rate with the tangential path velocity. The 3D laser scanner used

for the measurements has a resolution of 20 microns. The wall thicknesses are measured at sharp curvatures. The nominal wall thickness is 0.65 mm and it is calculated by assuming that the cross sectional area keeps constant at the nozzle and at the printed filament. The surfaces above in Figure 5.5 show the same sharp curvatures of two parts with constant and synchronized extrusion rate. The surfaces below are taken from the point, where the layer starts and begins. The excessive deposition can be seen as a result of a thicker wall thickness of the part printed with the constant extrusion rate.

5.4 Temperature Model Validation

The temperature model is validated by comparing the experimental results against the simulation results. The heating system and the controller are implemented as it's modeled in Chapter 4. The only input provided to the heating system is the extrusion rate commands at each sampling time. The feedback is provided by the thermistor (temperature sensor) located in the aluminum block. The controller parameters are calculated according to the design requirements and extrusion rate values. The aim is to keep the printing temperature as constant as possible, while the extrusion rate fluctuates.

The controller parameters change throughout the process due to the fluctuations in the extrusion rate profile. However, the amplitude of the fluctuations is small for this particular application. The thermal mass of the aluminum block is bigger than the thermal mass of the

filament material that is flowing through the heating zone at a certain time. This results in a slight change in the controller parameters.

A sample comparison of constant extrusion rate and synchronized extrusion rate profiles for one layer of print are shown in Figure 5.6. The tangential velocities for both of the case are first optimized without violating the linear drives' and extruder's limits. As the toolpath and the limits are the same for both of the cases, the tangential velocity is also the same. The current commands generated from the controller are also recorded to see the difference between the constant extrusion rate and synchronized extrusion rate cases. The current supplied to the heater remains the same, where the extrusion rate is kept constant.

It can be seen in Figure 5.6b that the extrusion rate decreases at sharp curvatures, where the tangential path velocity drops. Fluctuations in the current commands are expected in order to compensate the fluctuations in the temperature response because of the varying extrusion rate commands. This shows that the current supplied to the heater is adaptively reduced to maintain a constant printing temperature at 210°C.

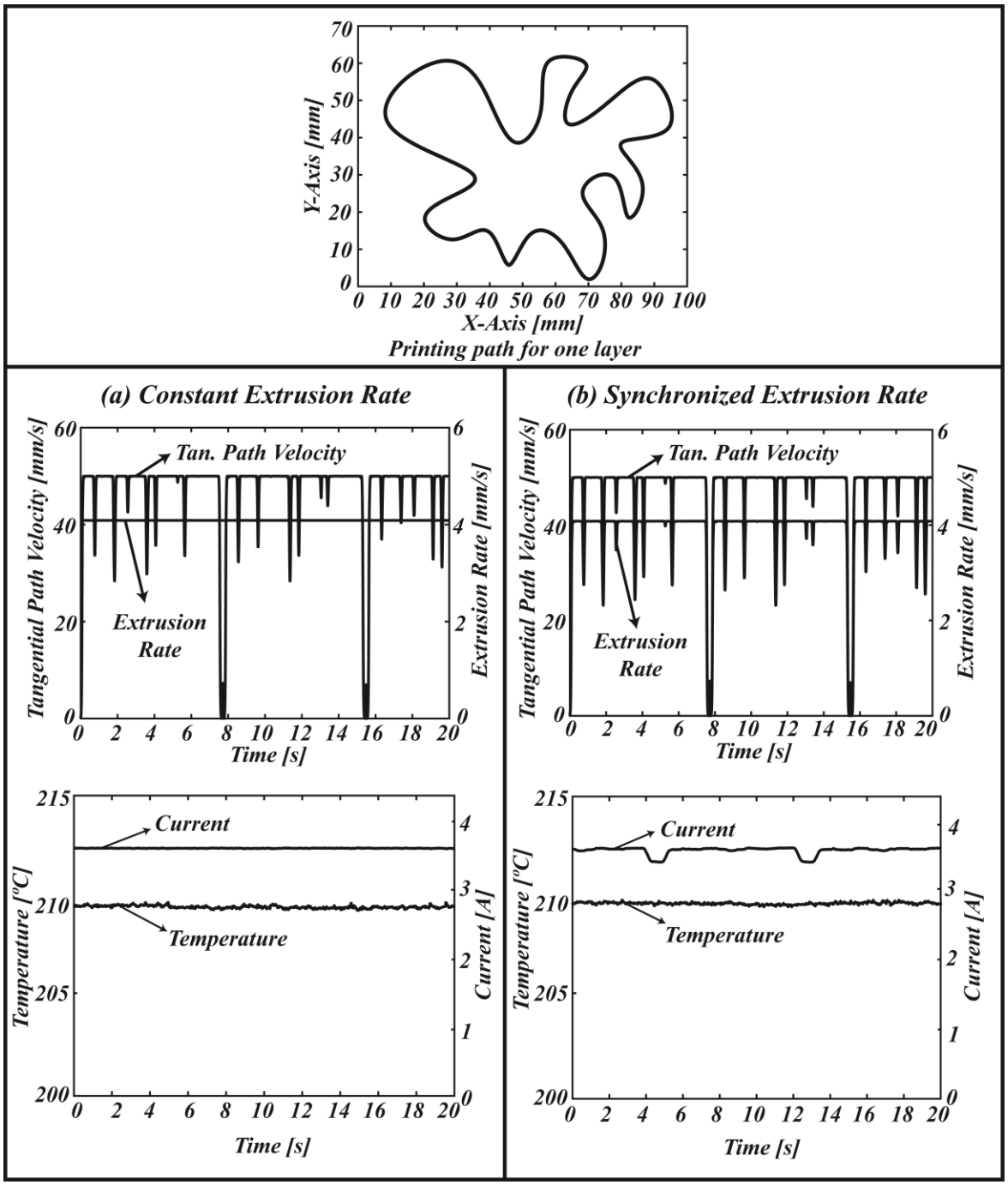

Figure 5.6 Comparison of Experimental Results Printed with Constant Extrusion Rate (a) and Synchronized Extrusion Rate (b)

5.5 Conclusions

In this chapter, experimental setup is introduced as the open architecture, in-house built fused deposition machine. Furthermore, the method proposed for the extrusion rate profile in Chapter 3 is used to print a part with synchronized extrusion rate. The temperature model is validated by comparing the simulation and experimental results against each other.

It can be seen that there is an improvement in the deposition profile when the method for the extrusion rate profile is used. Advancing the deposition profile makes the surface finish quality of the printed part better, where there is no excessive material deposition and material accumulation at critical points of the printed part.

Chapter 6: Conclusions

6.1 Conclusions

In this thesis, an off-line process planning and on-line process control technique for FDM operations is presented. The proposed novel method leads to a more homogeneous material deposition profile under constant material temperature during the printing process.

The process planning is needed to regulate the material deposition as a function of path velocity, which is currently not practiced. At the sharp corners and high curvatures of the toolpath, the printing table tends to make a full stop or slow-down, while the extruder continued to deposit the material at a constant rate. This will result in excessive material deposition at the curved tool-path locations as the extruder head will spend more time at these locations. A relation between the extrusion rate, the toolpath and tangential path velocity is established in this thesis. An extrusion rate profile is generated in synchronous with the tangential path velocity while considering the tool-path geometry and machine capabilities. The synchronised extrusion rate with the tangential velocity profile has been tested by printing a part with high curvatures and sharp corners. The same part is printed with a constant extrusion rate. It is shown that the part has equally and homogeneously distributed material deposition profile with a better surface finish quality.

When the filament mass transfer rate changes in the extrusion chamber, the heat must be regulated to achieve a constant temperature on the extruded material. The current systems use constant extrusion rate, hence the heater operates in an on-of fashion just to compensate for the heat losses monitored by the temperature sensor. This thesis presents a pole placement temperature controller whose parameters are adapted to varying filament extrusion rate in the heater chamber. It is shown that the temperature of the extruded filament is kept at the desired level as the extrusion rate (i.e. mass transfer in the heater) changes, which leads to more uniform material properties during the printing process.

6.2 Future Research Directions

Future research directions can be pursued in order to improve the process and the quality of the printed parts. The extrusion system used in this thesis and in most of the FDM machines operates in an open loop environment, where there is no actual extrusion rate feedback sensor. The stepper motor which feeds the filament also operates in an open loop fashion, hence slippage and velocity changes under the external disturbances are neglected. A servo motor with a velocity feedback can improve the extrusion rate control, which is expected to improve the printing rate in comparison to current, open loop step motor driven material delivery systems.

The proposed model has been experimentally validated in printing thermoplastic materials. However, the model is expected to lead to improved metal printing operations used in biomechanical implants, gas turbine and automotive parts using laser or electron – beam

systems. The metal printing process is more complex where the high-energy delivery, rapid cooling and energy losses, the distribution of temperature around the melt pool will bring extra challenges in process modeling and control.

Bibliography

[1] Crump, S.S., *Apparatus and method for creating three-dimensional objects*. 1992, Google Patents.

[2] Ma, W. and P. He, *Adaptive slicing and selective hatching strategy for layered manufacturing.* Journal of Materials Processing Technology, 1999. **89-90**: p. 191-197.

[3] Hildebrand, K., B. Bickel, and M. Alexa, *Orthogonal slicing for additive manufacturing.* Computers and Graphics (Pergamon), 2013. **37**(6): p. 669-675.

[4] Gibson, I., D. Rosen, and B. Stucker, *Additive manufacturing technologies: 3D printing, rapid prototyping, and direct digital manufacturing*. 2014: Springer.

[5] Ma, W., W.C. But, and P. He, *NURBS-based adaptive slicing for efficient rapid prototyping.* CAD Computer Aided Design, 2004. **36**(13): p. 1309-1325.

[6] Luo, R.C. and Y. Ma. *A slicing algorithm for rapid prototyping and manufacturing*. in *Robotics and Automation, 1995. Proceedings., 1995 IEEE International Conference on*. 1995. IEEE.

[7] Panhalkar, N., R. Paul, and S. Anand, *Increasing Part Accuracy in Additive Manufacturing Processes Using a k-d Tree Based Clustered Adaptive Layering.* Journal of Manufacturing Science and Engineering, 2014. **136**(6): p. 1-10.

[8] Ghazanfari, A., Li, W., Leu, M.C., and Landers, R.G., *Optimal Rastering Orientation in Freeform Extrusion Fabrication Processes*. in *International Solid Freeform Fabrication Symposium*. 2015: p. 1324-1333.

[9] Kim, C.Y., Cuaron, A., Perez M.A., Espalin, D., MacDonald, E. and Wicker, R.B., *Cooperative Fabrication Methodology for Embedding Wireon Curved Surfaces.* SFF Symposium, 2014: p. 185-196.

[10] Vatani, M., A. Rahimi, and F. Brazandeh, *An enhanced slicing algorithm using nearest distance analysis for layer manufacturing.* Proceeding of World Academy of Science, Engineering and Technology, 2009. **3**(25): p. 721-726.

[11] Heller, B., D. Smith, and D. Jack. *Effect of Extrudate Swell, Nozzle Shape, and Convergence Zone on Fiber Orientation in Fused Deposition Modeling Nozzle Flow*. in *International Solid Freeform Fabrication Symposium*. 2015.

[12] Erkorkmaz, K., *Optimal trajectory generation and precision tracking control for multi-axis machines*. PhD Thesis, University of British Columbia, 2004.

[13] Wang, F.-C. and D. Yang, *Nearly arc-length parameterized quintic-spline interpolation for precision machining.* Computer-Aided Design, 1993. **25**(5): p. 281-288.

[14] Wang, F.-C., Wright P.K., Barsky B.A., and Yang D.C.H., *Approximately arc-length parametrized C3 quintic interpolatory splines.* Journal of Mechanical Design, 1999. **121**(3): p. 430-439.

[15] Farouki, R.T. and S. Shah, *Real-time CNC interpolators for Pythagorean-hodograph curves.* Computer Aided Geometric Design, 1996. **13**(7): p. 583-600.

[16] Erkorkmaz, K. and Y. Altintas, *Quintic spline interpolation with minimal feed fluctuation.* Journal of manufacturing science and engineering, 2005. **127**(2): p. 339-349.

[17] Bellini, A., S.u. Güçeri, and M. Bertoldi, *Liquefier Dynamics in Fused Deposition.* Journal of Manufacturing Science and Engineering, 2004. **126**(2): p. 237-246.

[18] Agarwala, M.K., Jamalabad, V.R., Langrana, N.A., Safari, A., Whalen P.J. and Danforth S.C., *Structural quality of parts processed by fused deposition.* Rapid Prototyping Journal, 1996. **2**(4): p. 4-19.

[19] Yardimci, A.M., Hattori, T., Guceri S. and Danforth S.C., *Thermal Analysis of Fused Deposition*, in *Solid Freeform Fabrication Symposium*. 1997.

[20] Yardimci A.M., M. and S. Güçeri, *Conceptual framework for the thermal process modelling of fused deposition.* Rapid Prototyping Journal, 1996. **2**(2): p. 26-31.

[21] Ramanath, H., et al., *Melt flow behaviour of poly-ε-caprolactone in fused deposition modelling.* Journal of Materials Science: Materials in Medicine, 2008. **19**(7): p. 2541-2550.

[22] Mostafa, N., Syed, H.M., Igor, S. and Andrew, G., *A study of melt flow analysis of an ABS-Iron composite in fused deposition modelling process.* Tsinghua Science & Technology, 2009. **14**: p. 29-37.

[23] Liang, J., J. Chan, and E. Wong, *Effects of operation conditions and die angles on the pressure losses in capillary flow of polystyrene melt.* Journal of Materials Processing Technology, 2001. **114**(2): p. 118-121.

[24] Weiss, B.M., *Closed-Loop Control of a 3D Printer Gantry*, in *Mechanical Engineering*. 2014, University of Washington.

[25] Bouhal, A., et al., *Tracking Control and Trajectory Planning in Layered Manufacturing Applications.* IEEE Transactions on industrial electrnoics, 1999. **46**(2): p. 445-451.

[26] Han, W., et al., *Tool Path-Based Deposition Planning in Fused Deposition Processes.* Journal of Manufacturing Science and Engineering, 2002. **124**(2): p. 462-462.

[27] Han, W. and M.A. Jafari, *Coordination control of positioning and deposition in layered manufacturing.* IEEE Transactions on Industrial Electronics, 2007. **54**(1): p. 651-659.

[28] Crockett, R.S., *The liquid-to-solid transition in stereodeposition techniques.* PhD Thesis, University of Arizona, 1997.

[29] Middleman, S., *Modeling axisymmetric flows: dynamics of films, jets, and drops*. 1995: Academic Press.

[30] Bellini, A. and S. Güçeri, *Mechanical characterization of parts fabricated using fused deposition modeling.* Rapid Prototyping Journal, 2003. **9**(4): p. 252-264.

[31] Thomas, J. and J. Rodríguez. *Modeling the fracture strength between fused deposition extruded roads*. in *Proceedings of the 11th Solid Freeform Fabrication Symposium*. 2000.

[32] Bellini, A., *Fused deposition of ceramics: a comprehensive experimental, analytical and computational study of material behavior, fabrication process and equipment design*. PhD Thesis, Drexel University, 2002.

[33] Hu, D. and R. Kovacevic, *Sensing, modeling and control for laser-based additive manufacturing.* International Journal of Machine Tools and Manufacture, 2003. **43**(1): p. 51-60.

[34] Simchi, A., *Direct laser sintering of metal powders: Mechanism, kinetics and microstructural features.* Materials Science and Engineering: A, 2006. **428**(1): p. 148-158.

[35] Mani, M., Lane, B., Donmez, A., Feng, S., Moylan, S., and Fesperman, R., *Measurement science needs for real-time control of additive manufacturing powder bed fusion processes.* National Institute of Standards and Technology, Gaithersburg, MD, NIST Interagency/Internal Report (NISTIR), 2015. **8036**.

[36] Ji, L. B., and Tian R. Z., "Finite element simulation of temperature field in fused deposition modeling." *Advanced Materials Research*. Vol. 97. Trans Tech Publications, 2010.

[37] Piegl, L. and W. Tiller, *The NURBS book*. 2012: Springer Science & Business Media.

[38] Heng, M. and K. Erkorkmaz, *Design of a NURBS interpolator with minimal feed fluctuation and continuous feed modulation capability.* International Journal of Machine Tools and Manufacture, 2010. **50**(3): p. 281-293.

[39] Sencer, B., Y. Altintas, and E. Croft, *Feed optimization for five-axis CNC machine tools with drive constraints.* International Journal of Machine Tools and Manufacture, 2008. **48**(7): p. 733-745.

[40] Sencer, B., *Smooth trajectory generation and precision control of 5-axis CNC machine tools*. PhD Thesis, University of British Columbia, 2009.

[41] Coleman, T., M.A. Branch, and A. Grace, *Optimization toolbox.* For Use with MATLAB. User's Guide for MATLAB 5, Version 2, Relaese II, 1999.

[42] Erkorkmaz, K., Y. Altintas, and C.-H. Yeung, *Virtual computer numerical control system.* CIRP Annals-Manufacturing Technology, 2006. **55**(1): p. 399-402.